


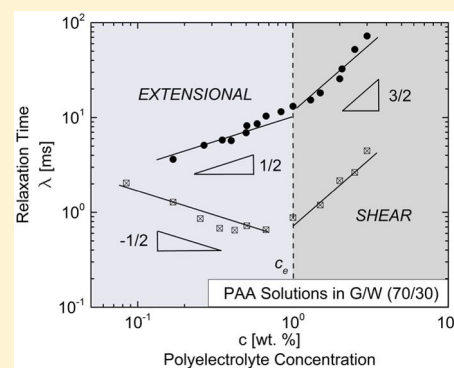
Extensional Relaxation Time, Pinch-Off Dynamics, and Printability of Semidilute Polyelectrolyte Solutions

Leidy Nallely Jimenez, Jelena Dinic, Nikhila Parsi, and Vivek Sharma*

Department of Chemical Engineering, University of Illinois at Chicago, Chicago, Illinois 60607, United States

Supporting Information

ABSTRACT: Quantitative studies of capillary-driven thinning and pinch-off dynamics of semidilute polyelectrolyte solutions, and their response to extensional flows, typically encountered in drop formation applications, are relatively rare and are the focus of this contribution. Here the pinch-off dynamics and extensional rheology of two model polyelectrolytes—poly(sodium 4-styrenesulfonate) (NaPSS) and poly(acrylic acid) (PAA)—in two different solvents are characterized by using Dripping-onto-Substrate (DoS) rheometry. Unlike shear relaxation time that decreases with increase in concentration in the unentangled, semidilute solutions, the extensional relaxation time of PAA solutions increases with an exponent of 1/2, and the entangled semidilute solutions also exhibit a stronger concentration dependence of 3/2. In contrast, the extensional relaxation time is not measurable for the unentangled, semidilute aqueous NaPSS solutions, though entangled NaPSS solutions show concentration-dependent values. The experiments and analysis described herein elucidate how the interplay of stretching due to electrostatics and hydrodynamics influences extensional rheology response and printability of polyelectrolyte dispersions.



INTRODUCTION

Biological macromolecules like proteins, DNA, and polysaccharides, as well as many industrial polymers, are classified together as polyelectrolytes, for in solution the repeat units in their backbone are decorated with disassociated, charge-bearing ionic groups, surrounded by a cloud of counterions.^{1–9} A large number of polyelectrolytes are processed or used as rheology modifiers in aqueous sprayable dispersions with applications including paints, pharmaceuticals, fertilizers, pesticides, and cosmetics.^{9,10} Many printed bioassays, DNA microarrays, photovoltaics, electronics, and organs involve the processing of inks containing polyelectrolytes.^{11,12} Understanding of and control over the influence of added polyelectrolytes on complex free surface flows encountered in printing^{13–15} (inkjet, gravure, etc.) as well as spraying, dispensing, and microfluidic drops (or emulsion) formation are both scientifically and technologically significant problems.^{11–16} The aforementioned drop formation techniques all involve the formation of columnar necks that undergo capillary-driven instability, thinning, and pinch-off.^{14–19} Streamwise velocity gradients with strong extensional kinematics develop in a fluid neck undergoing capillary-driven thinning, and therefore the response to extensional flow field influences printability, jettability, sprayability, or spinnability.^{19–21} Even though the Trouton ratio, Tr (the ratio of extensional to shear viscosity), is only three for Newtonian fluids, the solutions of neutral polymer solutions can display significantly high values ($Tr = 10^2–10^5$).^{19–25} Even though a large number of experimental and theoretical studies character-

ize the response of polyelectrolyte solutions to shear flow (summarized in reviews),^{1–6,26–29} only a countable few studies^{30–45} characterize their extensional rheology response. Among these, the experimental studies primarily include the stagnation-point flow experiments carried out by the Bristol group^{30–33} and by Dunlap and Leal^{34,35} in the 1980s. Quantitative studies of capillary-driven thinning and pinch-off dynamics of semidilute polyelectrolyte solutions, and their response to extensional flows encountered in printing, spraying, and coating applications, are relatively rare and are the focus of this contribution.

Stretching due to electrostatic interactions leads to more expanded conformations for polyelectrolytes, leading to a significantly low overlap concentration in contrast to neutral polymers. Practically, therefore, for the same weight fraction of added macromolecules, polyelectrolytes can boost shear viscosity more significantly than neutral polymers. The contrast between dynamics of charged and neutral polymers in solution is manifested in experiments^{26,27} as well as theory and simulations^{2–7,28} in the measurements of shear viscosity and relaxation time (often extracted from the onset of shear thinning^{27,29}). In contrast to shear flows that weakly perturb macromolecular coils, strong extensional flow fields can unravel the chains,^{19,46–50} leading to a pronounced coil–stretch transition for flexible neutral polymers.^{46–51} Previous

Received: January 21, 2018

Revised: May 21, 2018

Published: July 9, 2018

Table 1. Scaling Relationships for Shear Relaxation Time and Shear Viscosity Describe Concentration-Dependent Response Expected for Polyelectrolyte and Neutral Polymer Solutions

semidilute solutions	blob model	polyelectrolyte low salt	polyelectrolyte high salt	neutral polymer good solvent
unentangled relaxation time	$\lambda \sim \xi^{-3}c^{-2}N^2$	$c^{-1/2}N^2$	$c^{1/4}c_s^{-3/4}N^2$	$c^{1/4}N^2$
unentangled viscosity	$\eta \sim \xi^{-3}c^{-1}N$	$c^{1/2}N$	$c^{5/4}c_s^{-3/4}N$	$c^{5/4}N$
entangled relaxation time	$\lambda \sim \xi^{-6}c^{-3}N^3$	c^0N^3	$c^{3/2}c_s^{-3/2}N^3$	$c^{3/2}N^3$
entangled viscosity	$\eta \sim \xi^{-9}c^{-3}N^3$	$c^{3/2}N^3$	$c^{15/4}c_s^{-9/4}N^3$	$c^{15/4}N^3$

extensional flow studies on dilute solutions of charged polymers show either a rigid-rod-like continuous extension or a sharp coil–stretch transition depending upon the molecular weight, added salt type, and salt concentration.^{30–33,35,36} Although polyelectrolyte chains are partially stretched by intramolecular electrostatic repulsion of the charge-bearing segments, the electrostatic interaction in semidilute solutions gets screened beyond a correlation length, and macromolecules can be described as a swollen Gaussian chain of blobs that undergoes Rouse relaxation. As both correlation blob size and the size of coils decrease with increasing concentration,^{1–4} the shear relaxation time decreases with concentration in semidilute unentangled polyelectrolyte solutions,^{26,27} and shear viscosity exhibits a weaker concentration dependence than observed for neutral polymers (see the next section). Determining the concentration-dependent variation of extensional relaxation time and extensional viscosity of semidilute polyelectrolyte solutions is one of the primary goals of this study.

In this contribution, we characterize the shear and extensional rheology response of salt-free solutions of two polyelectrolytes in two solvents: water and water–glycerol mixture containing 70 vol % glycerol (higher viscosity, but with a lower dielectric constant than water). We utilize Dripping-onto-Substrate (DoS) rheometry protocols to probe how the presence of charge influences the capillary-driven thinning and pinch-off behavior and extensional relaxation time for semidilute solutions of two polyelectrolytes: poly(sodium 4-styrenesulfonate) (NaPSS) and poly(acrylic acid) (PAA).⁵² We have recently shown that the DoS rheometry protocols that rely on the visualization and analysis of capillary-driven thinning and pinch-off dynamics of a stretched liquid bridge formed between a nozzle and a sessile drop on a substrate can be used for measuring extensional viscosity (transient $\eta_E^t = \eta_E(\dot{\epsilon}, \epsilon, t)$ as well as steady, terminal extensional viscosity, η_E^∞) and extensional relaxation time.^{52–54} Here we aim to investigate the concentration-dependent variation in extensional relaxation time and pinch-off dynamics for unentangled and entangled semidilute polyelectrolyte solutions. We identify the unentangled and entangled semidilute regimes from the steady shear viscosity versus concentration plots. While the shear and extensional relaxation time of uncharged polymers always increases with concentration in the semidilute unentangled and entangled solutions,⁵⁵ the shear relaxation time of semidilute polyelectrolyte solutions decreases with concentration for the unentangled solutions and shows a concentration-independent value for entangled systems.^{3,4,26,27,29} The concentration dependence of extensional relaxation time of both unentangled and entangled semidilute polyelectrolyte solutions is characterized herein for the first time. The experiments and analysis described herein seek an understanding of how the interplay of stretching due to electrostatics and stretching due to hydrodynamics control the

extensional rheology response, drop formation dynamics, and ultimately printability of polyelectrolyte solutions.

■ BACKGROUND THEORY FOR SHEAR VISCOSITY AND SHEAR RELAXATION TIME

According to the scaling theories, the shear relaxation dynamics of both charged and uncharged polymers in semidilute solutions can be described using the composite Rouse–Zimm model or the blob model.^{1–4,28,55–57} Even though the original Zimm paper⁵⁸ developed for single chain hydrodynamics considered only the hydrodynamic interactions (HI), it is well established that excluded volume interactions can be quantitatively incorporated. The Zimm model^{46,55,58,59} (with EV and HI included) provides accurate predictions for the macromolecular dynamics in dilute solutions. In contrast, the original Rouse model^{46,59,60} (that neglects both EV and HI effects) captures the dynamics in unentangled melts. In blob models used for describing semidilute solution dynamics, the excluded volume (EV) and/or hydrodynamic (and in the charged systems, additional electrostatic) interactions are assumed to play a predominant role below a length scale shorter than the blob size, $\xi \approx g^{\nu}b$, where g is the number of segments and b is the size of each of the N segments in the chain. The size of macromolecules in a dilute solution can be described as $R \propto N^{\nu}b$, and the exponent $\nu = 1/2$ for neutral polymers in theta solvent and $\nu = 3/5$ for good solvent (0.588 according to the renormalization theories), and $\nu = 1$ for highly charged polyelectrolytes (salt-free). In the blob model, Zimm-like dynamics apply at length scales $r < \xi$, as the chain does not feel the presence of other chains. On length scales larger than the blob size, $r > \xi$ the chain effectively behaves like a Gaussian chain of N/g blobs, which displays Rouse-like dynamics due to screened interactions. Relaxation time on these length scales can be described using the Rouse model according to the equation $\lambda_{\text{chain}} \approx \lambda_{\xi}(N/g)^2$, where $\lambda_{\xi} \approx \eta_s \xi^3/kT$ is the time scale associated with Zimm relaxation within the blob. Using these formulas, together with the understanding that the number of monomers in the correlation blob is $g \sim c\xi^3 \sim c^{-1/(3\nu-1)}$, leads to a concentration-dependent relaxation time⁵⁵ of the form $\lambda \propto c^m$ with exponent $m = (2 - 3\nu)/(3\nu - 1)$.

In neutral polymers, the scaling exponent for concentration-dependent relaxation time equals $m = 1/4$ for $\nu = 3/5$ (or $m = 0.31$ for $\nu = 0.588$) for a good solvent and equals $m = 1$ if EV interactions are screened or absent. For the case of polyelectrolytes, the exponent turns out to be $m = -1/2$ (if $\nu = 1$ or strong electrostatic-induced stretching is assumed), and therefore shear relaxation time increases on dilution in semidilute, unentangled polyelectrolyte solutions. In the semidilute, unentangled solutions of both neutral and charged polymers, the shear modulus can be estimated as $G \sim cN^{-1}$, and as shear viscosity is determined using $\eta \sim G\lambda$, the scaling exponents listed in Table 1 follow. In the entangled solutions, the longest relaxation time of the chains can be estimated using reptation theory by assuming that the dynamics below the

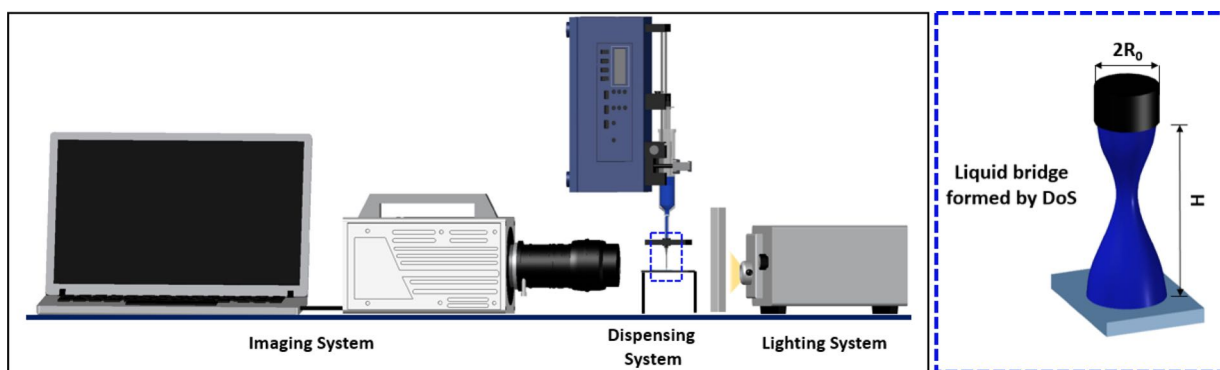


Figure 1. Schematic for Dripping-onto-Substrate (DoS) rheometry. The DoS setup includes a dispensing system and an imaging system for visualizing and recording the capillary thinning and pinch-off dynamics of the liquid neck formed by dispensing a discrete amount of fluid onto a substrate.^{52–54} The dispensing system includes a syringe pump that releases a finite volume of fluid through a nozzle placed height H above the clean glass substrate. The imaging system includes a light source, a diffuser, and a high-speed camera (with magnifying lenses) connected to a laptop.

correlation blob size are Zimm-like, below entanglement length are Rouse-like, and the entanglement length itself is proportional to the correlation blob size. The relaxation time of entangled polyelectrolyte chains shows a scaling exponent of zero, and by defining $G \sim \xi^{-3}$, the scaling exponent of 3/2 is obtained for both shear viscosity and modulus.

MATERIALS AND EXPERIMENTAL METHODS

Representative Polyelectrolyte Solutions. Poly(sodium 4-styrenesulfonate) (NaPSS) and poly(acrylic acid) (PAA) of $M_w = 1000$ and 450 kDa, respectively, were purchased from Sigma-Aldrich and were used without further purification as representative systems for studying polyelectrolyte behavior. NaPSS is chosen as a model polyelectrolyte for it is one of the most well-studied polyelectrolytes, and it is used in fuel cells and organic photovoltaics (as PEDOT-PSS),^{61,62} water softening, and medicine.⁶³ Poly(acrylic acid) is used in diverse applications ranging from enhanced oil recovery⁶⁴ to thickeners in food processing and cosmetics,⁶⁵ wherein the charge on the polyelectrolytes is employed to coagulate, flocculate, disperse, or thicken the medium. Historically, aqueous solutions of PAA were the earliest polyelectrolyte solutions for which viscosity measurements were reported by Staudinger,⁶⁶ Markovitz and Kimball,⁶⁷ and Katchalsky and Eisenberg,⁶⁸ among others, and the early studies provided the initial insights into the effect of pH, ionic content, molecular weight, concentration, etc., on polyelectrolyte size and rheology. Polyelectrolyte solutions were prepared in polyethylene bottles, and for all the concentrations investigated, the polyelectrolytes used in this study were found to form single phase, homogeneous dispersions. Dry polymer powder was slowly added to deionized water, and the polymer solution was left on a roller for 5 days to ensure complete mixing and to minimize chain breakup associated with high deformation rate mixing flows. Additional solutions were prepared in 70% glycerol per volume glycerol/water mixtures.

Shear Rheology Measurements. The shear rheology response of the polyelectrolyte solutions was characterized using a concentric cylinder (double gap) Couette cell on an Anton Paar MCR 302 rheometer (torque range 10^{-5} –200 mN·m) at 25 °C. The steady shear viscosity, $\eta(\dot{\gamma}) \equiv \tau/\dot{\gamma}$ was computed from the measured shear stress, τ , resulting from a specified applied shear rate, $\dot{\gamma}$. Steady shear viscosity values were measurable for the aqueous polyelectrolyte solutions in the shear rates in the range of 1 – 10^3 s⁻¹. Additional data at higher shear rates were acquired using a microfluidic channel device, called the Viscometer-Rheometer-on-Chip (VROC, Rheo-Sense Inc., San Ramon, CA). Each microfluidic channel contains a series of flush-mounted pressure sensors, each measuring $800 \times 800 \mu\text{m}^2$, located along the centerline of the channel (Type A05 chipset, with channel width, $w = 3.02$ mm; height, $d = 50 \mu\text{m}$ and maximum

pressure, $P_{\text{max}} = 10$ kPa). In a typical experiment, the flow rate, Q , is varied using a syringe pump, and the microfluidic device measures the pressure drop in the channel as a function of the flow rate. The pressure drop, ΔP , required to drive the flow is related to the wall shear stress, τ_w , by the expression $\Delta Pwd = 2L(w + d)\tau_w$, and the nominal wall shear rate, $\dot{\gamma}_{Nw}$, associated with fully developed laminar flow of a Newtonian fluid is $\dot{\gamma}_{Nw} = 6Q/wd^2$. For a non-Newtonian, shear thinning fluid, the velocity profiles in the channel are not parabolic, and the resulting plot of ΔP versus Q is nonlinear. In this case, the true wall shear rate $\dot{\gamma}_w$ was computed using the Weissenberg–Rabinowitsch–Mooney (WRM) equation⁶⁹ and was used for computing steady shear viscosity. All the VROC measurements were carried out at room temperature, 22–25 °C.

Dripping-onto-Substrate (DoS) Rheometry. The DoS rheometry setup, shown schematically in Figure 1, was utilized for characterizing pinch-off dynamics and the extensional rheology response. The setup comprises of a dispensing system and an imaging system. A finite volume of polyelectrolyte solution is released from the nozzle onto a substrate to form a liquid bridge between the nozzle and the sessile drop formed on the surface. The nozzle used in this study has an outer diameter of $D_o = 2R_o = 1.27$ mm and an inner diameter of $D_i = 0.838$ mm), and the aspect ratio selected was kept constant at $H/D_o \approx 3$. The flow rate was also kept constant for all experiments ($Q = 0.02$ mL/min). As noted before,⁵³ the relatively slow release of drops onto a partial wetting substrate (spreading parameter $S < 0$ and contact angle $\theta < 90^\circ$) helps to decouple the neck thinning dynamics from the drop spreading dynamics, and if needed, the contact line of the sessile drop can be pinned by using a cylindrical plate as a substrate.

The imaging system consists of a light source with a diffuser and a high-speed camera (Fastcam SA3) with a train of lenses (Nikkor 3.1 x zoom (18–25 mm) lens, plus a macro lens) attached for obtaining images with high magnification and at high frame rate (8000–25 000 frames per second (fps)). The DoS videos were analyzed using ImageJ⁷⁰ and MATLAB using specially written codes for edge detection and for determination of neck radius as a function of time (codes and procedure are detailed in previous studies⁵³). As aqueous solutions wet the metal nozzle used in this study, the outer diameter of the nozzle, D_o , is used for scaling the neck diameter and also for determining the absolute pixel size per unit length. The typical size of the symbols chosen for all the radius evolution plots is of the same order as the error ($\sim 10 \mu\text{m}$) estimated by accounting for the resolution of the imaging systems and the analysis protocols. Although the pinch-off dynamics of simple fluids are dictated by a complex interplay of inertial, viscous, and capillary stresses,^{14–16,18,19} additional viscoelastic stresses associated with stretching and orientation of macromolecules arise in polymer solutions, leading to a measurable delay in pinch-off.^{21,40,71–81} The self-thinning analysis for DoS rheometry is based on the scaling laws and theories also used for

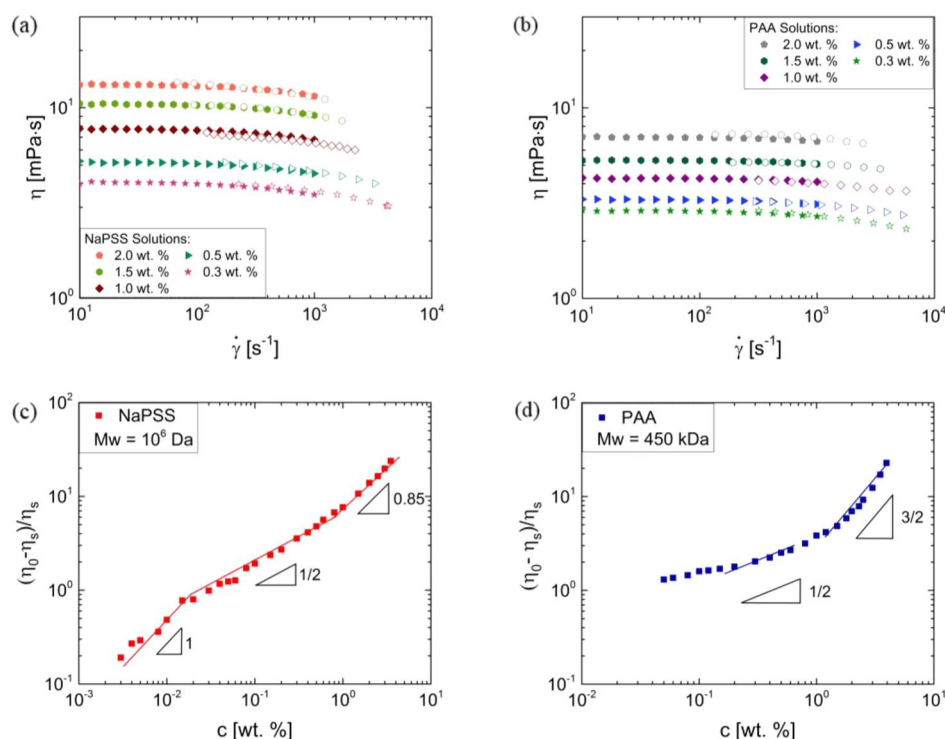


Figure 2. Shear rheology response of aqueous NaPSS and PAA solutions. (a) Steady shear viscosity as a function of shear rate of aqueous NaPSS solutions was measured using torsional rheometer (closed symbols) and microfluidic rheometer (open symbols). Viscosity increases with concentration. (b) Steady shear viscosity as a function of shear rate for aqueous PAA solutions exhibits a concentration-dependent increase. (c) Relative viscosity increment, $\eta_i = (\eta_0 - \eta_s)/\eta_s$, as a function of concentration for aqueous NaPSS solutions shows three scaling regimes: $\eta_i \propto c^1$ in the dilute regime, $\eta_i \propto c^{1/2}$ for the semidilute, unentangled regime, and $\eta_i \propto c^{0.85}$ in the entangled regime. (d) Relative viscosity increment as a function of concentration for aqueous semidilute solutions of PAA increases with $\eta_i \propto c^{1/2}$ in the unentangled and $\eta_i \propto c^{3/2}$ in the entangled regime. The transition in scaling in semidilute solution can be identified as entanglement concentration, c_e , and the value of $c_e = 1$ wt % for NaPSS and $c_e = 1.5$ wt % for PAA solutions.

analyzing neck thinning dynamics of stretched liquid bridges,^{19,40,73–77} including data sets obtained from the commercially available extensional rheometer called capillary breakup extensional rheometer (CaBER).^{80,81} The CaBER measurements rely on the visualization and analysis of neck thinning dynamics of a stretched liquid bridge formed by applying step strain to fluid confined between two parallel plates.^{19,80,81} As the step-strain itself requires around 50 ms, and the time to pinch-off for low-viscosity fluids including aqueous polyelectrolyte solutions is typically shorter, such measurements are not possible on CaBER.⁸¹ However, using DoS rheometry,^{52–54} the delayed pinch-off, relaxation time, and high extensional viscosity can be measured even for polymer solutions in low-viscosity solvents like water with $\eta = O(1$ mPa·s), and hence the use of DoS rheometry enables measurement of the extensional rheology response of aqueous polyelectrolyte solutions, even though similar measurements are inaccessible in the commercially available extensional rheometer.

RESULTS AND DISCUSSION

Shear Rheology of Aqueous NaPSS and PAA Solutions. The steady shear viscosity data as a function of shear rate are plotted for a range of concentrations for aqueous NaPSS solutions and aqueous PAA solutions in Figure 2a,b. Although aqueous solutions of both polyelectrolytes show nearly Newtonian response, the absolute viscosity values for aqueous NaPSS solutions are higher at matched concentrations, as NaPSS has a higher molecular weight and probably a higher charge fraction than PAA. The steady shear viscosity data measured using torsional rheometry (Anton Paar, MCR 302), which are shown with closed symbols, are supplemented

by additional data points (open symbols) acquired at higher shear rates using the microfluidic viscometer (m-VROC). The zero shear viscosity η_0 extracted from this data and solvent (water) viscosity value ($\eta_s = 0.89$ mPa·s) are used for computing the relative viscosity increment, $\eta_i = (\eta_0 - \eta_s)/\eta_s$, plotted for aqueous NaPSS and PAA solutions respectively in Figures 2c and 2d. For a range of concentrations, the relative viscosity increment of both aqueous NaPSS and PAA solutions shows the concentration dependence $\eta_i \propto c^{1/2}$ which is referred to as the Fuoss law.^{1–4,28,82,83} Scaling theories by Witten and Pincus,⁸⁴ Dobrynin, Colby, and Rubinstein,²⁸ and Muthukumar² capture the concentration dependence $\eta_i \propto c^{1/2}$ observed for semidilute, unentangled polyelectrolyte solutions in many studies.^{1–7,26–29,57,82–99} Defining the overlap concentration (c^*) as the polymer concentration for which the solution viscosity is exactly twice the solvent viscosity, the data sets yield $c^* \approx 0.02$ wt % for NaPSS and $c^* \approx 0.05$ wt % for PAA solutions. The intrinsic viscosity values estimated using $c^*[\eta] = 1$ are $[\eta]^{\text{NaPSS}} \approx 50$ dL/g and $[\eta]^{\text{PAA}} \approx 20$ dL/g, which are comparatively large in contrast to $[\eta]^{\text{PEO}} \approx 6$ dL/g measured for aqueous PEO solution (neutral polymer in good solvent, with $M_w = 1000$ kDa). The higher intrinsic viscosity values of aqueous solutions NaPSS ($M_w = 1000$ kDa) and PAA ($M_w = 450$ kDa) are due to larger pervaded volume of the electrostatically stretched chains.

In Figure 2c, below the overlap concentration, the aqueous NaPSS solutions show a dilute regime with a scaling of $\eta_i \propto c^1$ for $c < 0.02$ wt %, and for $c > 1$ wt % ($c_e = 50c^*$), a concentration dependence $\eta_i \propto c^{0.85}$ is observed. A similar

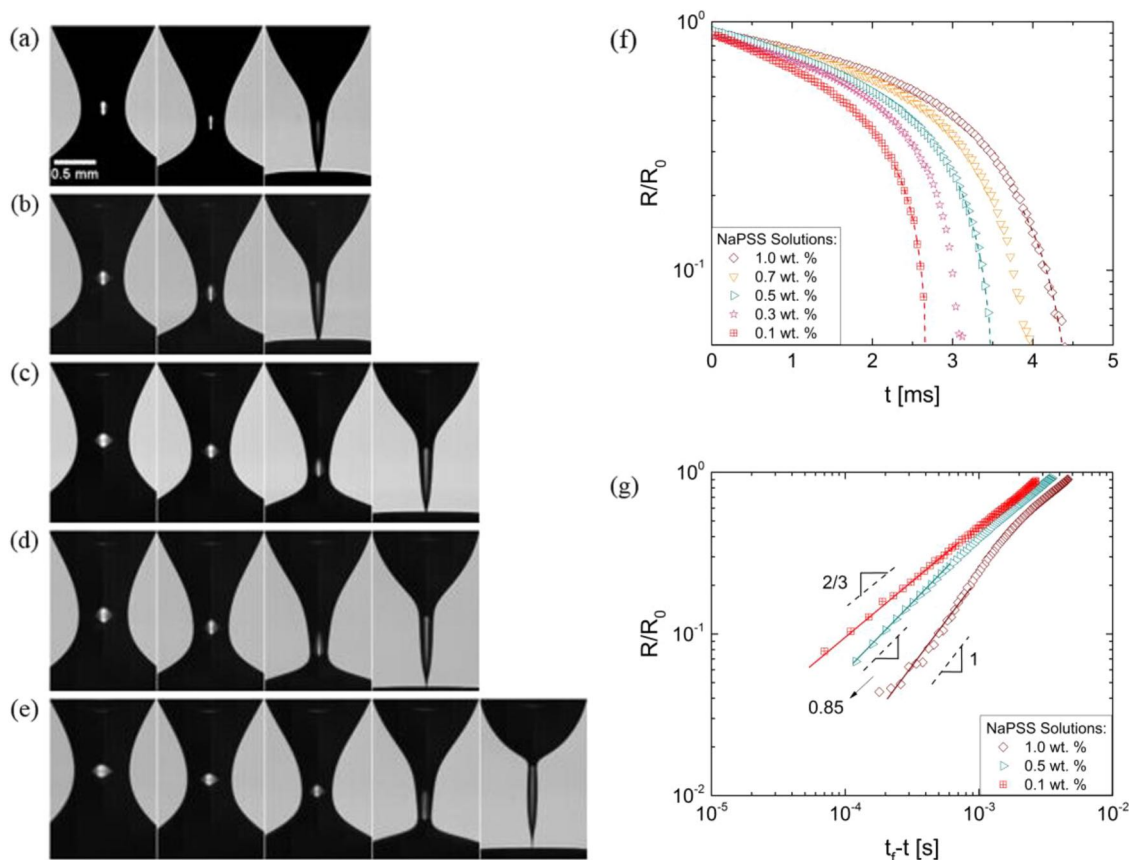


Figure 3. Characterizing capillary-driven thinning and pinch-off dynamics of unentangled aqueous NaPSS solutions ($M_w = 10^6$ Da) using the DoS rheometry technique. (a–e) Image sequences, 1 ms apart, acquired using 25 000 fps for solutions with $c = 0.1, 0.3, 0.5, 0.7,$ and 1 wt %, show a clear transition from the conical shape obtained at the lowest concentration of 0.1 wt % to a cone, connected to the sessile drop via a short, slender filament for 1 wt %. (f) Radius evolution over time for the aqueous NaPSS solutions obtained using DoS rheometry shown on a semilog plot shows concentration-dependent variation in both shape of the curves and the pinch-off time. (g) Radius evolution data replotted as a function of shifted time. The power law fits $R(t)/R_0 = A(t_f - t)^n$ for each data set show that the solution with lowest concentration, 0.1 wt %, shows an inertio-capillary response with $n = 2/3$ (conical shape) and at 1 wt %, the highest concentration shown, although $n = 1$, the slender cylindrical neck associated with visco-capillary response is observed as a filament between the cone and sessile drop, just before pinch-off.

power law regime with $\eta_i \propto c^{0.85}$ was observed in the data sets of Uzum et al.⁸⁶ for aqueous NaPSS solutions (M_w ranging from 4.2 to 2260 kDa) the power law regime, referred to as shoulder region is also observed in additional, older data sets including those from Prini et al.⁹⁵ ($M_w = 3.98$ kDa), Cohen et al.,^{96,97} and Oostwal et al.⁹⁸ ($M_w = 3.98$ kDa, viscosity values as cited²⁷), among others. The influence of polydispersity in molecular weight, variation in charge fraction and chain hydrophobicity, amount of dissolved carbon dioxide, and flaws in rheometric measurements (see detailed discussion in Boris and Colby²⁷) can all contribute to the measured concentration-dependent response. However, the data sets obtained by Boris and Colby²⁷ ($M_w = 1200$ kDa) as well as Chen and Archer⁹⁹ ($M_w = 262, 585, 801,$ and 1188 kDa) exhibit a $3/2$ power law for salt-free aqueous NaPSS solutions. The power law of $3/2$ is also observed for solutions of poly(methyl-2-vinylpyridinium chloride) (PMVP-Cl) random copolymer in ethylene glycol,^{29,100} sodium carboxymethyl cellulose aqueous solutions,¹⁰¹ and xanthan gum aqueous solutions.⁹³ The observed concentration dependence for aqueous NaPSS solutions is weaker than the scaling theory prediction of $\eta_i \propto c^{3/2}$ for entangled polyelectrolyte solutions made by Dobrynin, Colby, and Rubinstein^{3,4,26,28} as well as the prediction of $\eta_i \propto c^{1.7}$ obtained by Muthukumar.^{1,2,57,92} As shear viscosity is

relatively high ($\eta_i \sim O(10)$) and the behavior is distinct from the unentangled scaling (distinct response is also observed in extensional rheology measurements discussed later), we refer to this regime for $c > 1$ wt % ($c_e = 50c^* = 1$ wt %) as the entangled regime.

In contrast, the aqueous PAA solutions display the power law exponents of $\eta_i \propto c^{1/2}$ for $c > c^*$ (with $c^* = 0.05$ wt %) and $\eta_i \propto c^{3/2}$ for $c > 1.5$ wt % ($c_e = 30c^* = 1.5$ wt %) that correspond to the unentangled and entangled semidilute solution behavior expected from scaling theories^{3,4,28} and observed in previous experimental studies.^{26,27,29,101} Finally, while the semidilute regime spans only 1 order of magnitude beyond the overlap concentration, c^* , for the neutral polymers,^{55,59} the semidilute unentangled regime can span 1–4 orders of magnitude in concentration for low salt or salt-free strong polyelectrolytes, including the aqueous NaPSS solutions investigated in this study (see Figure 2).^{2–4,27–29} The lower M_w aqueous PAA solutions show the concentration dependence $\eta_i \propto c^{1/2}$ expected for semidilute, unentangled solutions over a narrower range of concentrations but display an outright transition to the concentration dependence of $\eta_i \propto c^{3/2}$ expected for entangled, semidilute polyelectrolyte solutions. In contrast, the neutral polymers do not display any regime with $\eta_i \propto c^{1/2}$, and for $c > c^*$, a stronger

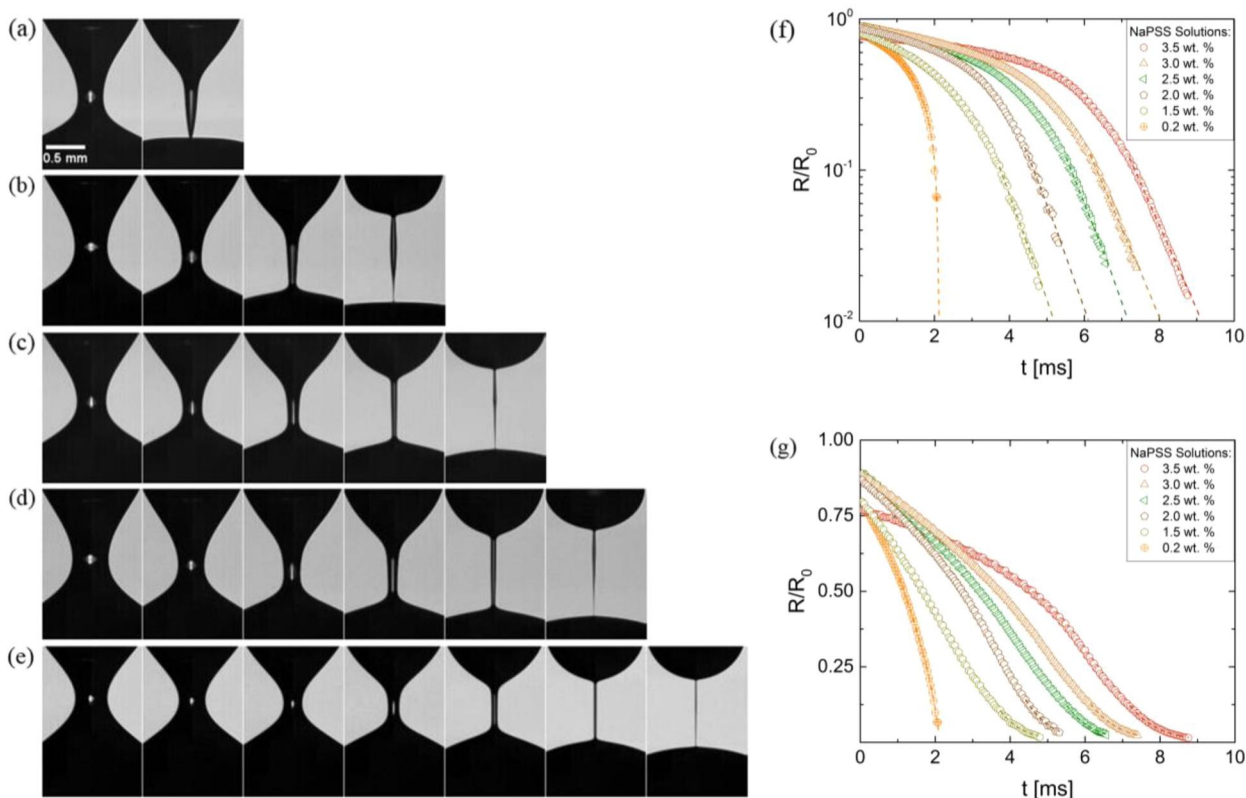


Figure 4. Characterizing capillary-driven thinning and pinch-off dynamics of entangled aqueous NaPSS solutions using DoS rheometry technique. (a–e) Image sequences, 1 ms apart, acquired at 25 000 fps, are shown for five concentrations $c = 0.2, 1.5, 2.5, 3,$ and 3.5 wt %. A progressive, concentration-dependent transition from conical shape (0.2 wt %) to a slender, cylindrical filament occurs, and pinch-off time gets longer. (f) Radius evolution plots as a function of time are shown on semilog axis for semidilute entangled solutions. The pinch-off event shifts to longer times with increase in concentration. The 0.2 wt % data is included to show inertio-capillary behavior. (g) Radius evolution data shown using a linear-linear axes for both scaled radius and time shows that the lowest concentration solution, 0.2 wt % (conical shape, connected to a cylindrical neck), exhibits the inertio-capillary response. The entangled NaPSS solutions, $c \geq 1.5$ wt % (slender cylindrical shape), exhibit an elastocapillary response in the small tail region which can be fit by eq 3 (fit is shown as line passing through data points).

concentration dependence $\eta_i \propto c^{1.3}$ is observed for semidilute, unentangled solutions.⁵⁵ Likewise, the scaling exponents observed for concentration-dependent viscosity data in Figure 2 are inconsistent with the exponents predicted in the high salt limit (see Table 1) and observed experimentally in polyelectrolyte solutions with added salt.^{27,102–104}

Pinch-Off Dynamics of Aqueous NaPSS Solutions Characterized Using DoS Rheometry. The snapshots showing progressive capillary-driven thinning and pinch-off of five representative aqueous semidilute NaPSS solutions ($M_w = 10^6$ Da, with $c = 0.1, 0.3, 0.5, 0.7,$ and 1 wt %) shown in Figure 3a–e were acquired using the DoS rheometry setup. The capillary-driven thinning leads to a conical-shaped neck, characteristic of inviscid fluid response, as observed for the lowest concentration samples (Figure 3a–c). The conical neck progressively disappears as the concentration-dependent viscosity of the polyelectrolyte solution rises (see Figures 3 and 4). The image sequence for the highest concentration solutions (1 wt %, Figure 3e) shows that the conical neck is connected to the sessile drop by a slender cylindrical filament in the late stage before pinch-off event. Figure 3f shows the radius evolution for the same range of concentrations as image sequences, and the dotted lines show power law fits $R(t)/R_0 = A(t_f - t)^n$, where t_f represents the pinch-off time. The data and power law fits are shown again in Figure 3g using time to pinch-off as the ordinate, such that pinch-off is approached

from right to left. For these semidilute, unentangled aqueous NaPSS solutions, the scaling exponents observed seem to lie between the two asymptotic values, i.e., $2/3 \leq n \leq 1$, as discussed next. The radius evolution data for the lowest concentration solution (0.1 wt %) can be characterized as inertio-capillary thinning response, described by the following expression:^{105,106}

$$\frac{R(t)}{R_0} = 0.8 \left(\frac{t_f - t}{t_R} \right)^{2/3} \quad (1)$$

Here, R_0 is the outer radius of the nozzle, and ρ and σ are the fluid density and surface tension, respectively. The characteristic time scale for inertio-capillary thinning^{14,17,107} called the Rayleigh time $t_R = (\rho R_0^3 / \sigma)^{1/2}$ is correlated to oscillation frequency of a drop of mass ρR_0^3 acted upon by surface tension that acts like an “effective spring constant”.

However, on examining the snapshots for the highest concentration solution included in this plot ($c = 1$ wt %), we find that a slender cylindrical neck appears as a filament that connects the cone to the sessile drop and exhibits the visco-capillary (VC) response before pinch-off, described by the following expression:^{19,108}

$$\frac{R(t)}{R_0} = 0.0709 \left(\frac{t_f - t}{t_{vc}} \right) \quad (2)$$

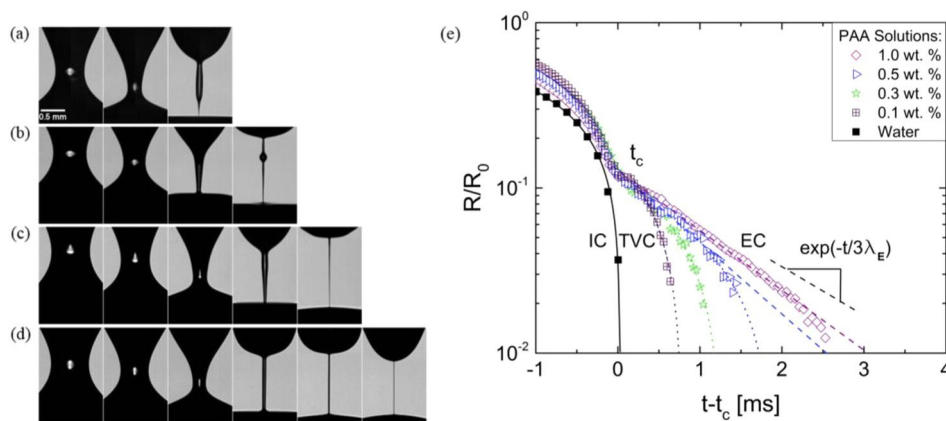


Figure 5. Capillary-driven thinning and pinch-off dynamics of aqueous PAA solutions in the semidilute, unentangled regime, characterized using DoS rheometry. (a–d) Image sequences with time step of 1 ms acquired at 25 000 fps, for $c = 0.1, 0.3, 0.5,$ and 1 wt %. Scale bar is for 0.5 mm. (e) Radius evolution plots as a function of shifted time are shown on a semilog plot for semidilute, unentangled solutions. The pinch-off event shifts to longer times with increase in concentration. The data for water is included to show the characteristic inertio-capillary response (fit with solid line). The time axis shifted using the transition time scale t_c highlights the change in thinning dynamics from the inertio-capillary regime to elastocapillary thinning behavior (fitted with dashed line). A third regime that follows the elastocapillary regime manifests just before pinch-off is henceforth christened as the terminal visco-capillary regime (fitted with dotted line).

Here the visco-capillary time $t_{vc} = \eta R_0 / \sigma$ represents the characteristic time scale for VC thinning. The relative importance of viscous and inertio-capillary effects can be evaluated by computing the Ohnesorge number, $Oh = t_{vc} / t_R = \eta / \sqrt{\rho \sigma R_0}$, which can be considered to be a suitable, dimensionless measure of viscosity. As the viscosity of semidilute, unentangled aqueous NaPSS solutions is quite low ($Oh < 0.1$), the conical shape of the neck is consistent with the expectations for a nearly inviscid fluid. However, due to sustained orientation and stretching of polyelectrolyte chains under extensional flow field, the higher concentration solutions exhibit higher effective viscosity, leading to the observed increase in the scaling exponents extracted here by analyzing the evolution of the minimum radius of the nonuniform neck. The nonuniform shape of the neck in these images (see Figure 3e) is strikingly different from the uniform slender, cylindrical necks observed for high viscosity, Newtonian fluids ($Oh > 1$) undergoing visco-capillary thinning.^{19,54} Henceforth, we would term this the terminal visco-capillary (TVC) regime. We introduce the qualifier terminal to denote the fact that the TVC regime arises due to the highly nonlinear, microstructural changes within the polymeric fluid under sustained extensional flow field, even though a visco-capillary response is not expected based on an estimate of Oh . Indeed, the apparent or effective viscosity value extracted from the TVC regime is usually higher than shear viscosity^{19,23,40,53,74,77} and is known as steady, terminal extensional viscosity.

However, the neck shape, overall life of the filament, and capillary thinning and pinch-off dynamics change quite dramatically at NaPSS concentrations beyond 1 wt % (or beyond the entanglement concentration, $c_e = 1$ wt %). The snapshots shown in Figure 4a–e and radius evolution data in Figure 4f show the progressive capillary-driven thinning and pinch-off of five aqueous NaPSS solutions ($M_w = 10^6$ Da, with $c = 1.5, 2.0, 2.5, 3.0,$ and 3.5 wt %) in the entangled regime. Although the elastocapillary regime is hard to visualize in the radius evolution data shown in the semilog plot (Figure 4f), an unmistakable slowing down in dynamics is observed just before pinch-off in a plot on linear–linear axis (shown in Figure 4g). The radius evolution profiles obtained here appear to be quite

similar to the radius evolution profiles obtained for entangled cellulose solution in an ionic liquid (cellulose behaves like a semiflexible polymer), reported by Haward et al. and obtained using CaBER measurements.¹⁰⁹

The radius evolution data in the elastocapillary regime is modeled by using the following expression based on a theory developed by Entov and Hinch:⁷⁴

$$\begin{aligned} \frac{R(t)}{R_0} &= \sum_i \left(\frac{g_i R_0}{2\sigma} \right)^{1/3} \exp[-t/3\lambda_i] \\ &\approx \left(\frac{G_E R_0}{2\sigma} \right)^{1/3} \exp[-t/3\lambda_E] \end{aligned} \quad (3)$$

Here g_i and λ_i are modulus and relaxation time that correspond to the i th mode of the relaxation spectrum.⁷⁴ For many polymer solutions,^{19,74} this response can be captured reasonably well by a single-exponential relaxation function, where G_E represents an apparent extensional modulus and λ_E represents the extensional relaxation time. The elastocapillary fits to the radius evolution data included in Figure 4 (shown as dotted lines) are used to extract the values of extensional relaxation time. The value of extensional relaxation time varies only weakly with concentrations, and all values are close to a nominal value of $\lambda_E = 0.2$ ms.

Pinch-Off Dynamics of Aqueous PAA Solutions Characterized Using DoS Rheometry. Although the radius evolution data show no visible elastocapillary response for aqueous NaPSS solutions in the semidilute, unentangled solutions ($c < 1.0$ wt %), the aqueous PAA solutions exhibit elastocapillary thinning, associated with an exponentially slow decrease in radius for the semidilute, unentangled regime $c > 0.2$ wt %. Figures 5a–d show image sequences with 1 ms between each image for a range of PAA concentrations in the semidilute, unentangled regime. The radius evolution data plotted in Figure 5e show a transition from the asymptotically approached inertio-capillary behavior before transitioning to the exponentially slow elastocapillary regime (fit by eq 3, see dashed line) for semidilute solutions $c > c^*$. The data sets are shifted to match the transition point, t_c , beyond which the

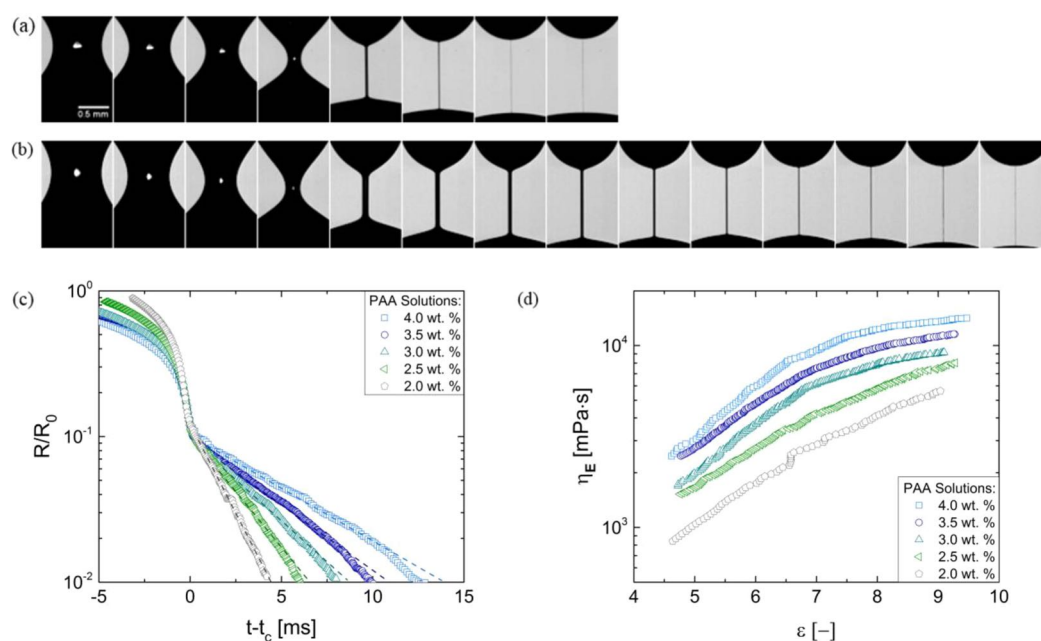


Figure 6. Capillary thinning dynamics for the aqueous PAA solutions in the semidilute entangled regime. (a, b) Image sequences for PAA solutions with 2 ms between each image using 25 000 fps, $c = 2, 4$ wt %. Scale bar is for 0.5 mm. (c) Radius evolution plot for the aqueous PAA solutions with the x -axis shifted to show an overlapping t_c . (d) Extensional viscosity as a function of Hencky strain for aqueous PAA solutions using DoS extensional rheometry. The extensional viscosity values are much higher than the shear viscosity values, and the Trouton ratio values range from 10^2 to 10^3 , showing significant strain hardening.

elastocapillary regime appears linear on a semilog radius evolution plot.

Additionally, for the lower concentration PAA solutions (0.1, 0.3, and 0.5 wt %), the last few points before pinch-off show a third regime, which can be captured by the terminal visco-capillary (TVC) thinning response that involves a fit with eq 2 with viscosity as the fit parameter. Again the TVC regime arises here due to microstructural changes within the fluid, even though visco-capillary thinning is not expected on the basis of the estimated value of Oh . The apparent viscosity deduced from the fit shown by dotted line in Figure 5e provides a measurement of the terminal, steady extensional viscosity, η_E^∞ . It has been pointed out before that η_E^∞ is arguably a true material response^{23,40,53,77} that depends on both molecular weight and polymer concentration, but not on extension rate or accumulated strain. The η_E^∞ values are reached before all the chains are completely stretched out^{71,77,110} and are quite sensitive to the extensibility parameter (ratio of fully extended chain size to unperturbed coil dimensions or $N^{1-\nu}$). Here the values of Trouton ratio $Tr^\infty = \eta_E^\infty/\eta_0$ equaling 25 and 40 are measured for the 0.3 and 0.5 wt % solutions, respectively. Dinic et al. showed⁵³ that the absolute values of extensional viscosity of the intrinsically semidilute, unentangled polymer solutions (PEO, $M_w = 10^6$ Da) are 250–3200 times higher than their zero shear viscosity, and in dilute PEO solutions, $Tr = 10^3$ – 10^6 can be observed. The value of the terminal Trouton ratio depends on the absolute value of zero shear viscosity as well as extensional viscosity, which itself depends on extensibility, $L = R_{\max}/\langle R^2 \rangle^{1/2} = N_K^{1-\nu}$ (defined as ratio of the size of a chain stretched by flow to the size of the unperturbed coil). As extensibility depends on both the value of exponent ν and the number of Kuhn segments, N_K (or molecular weight), neutral polymers are more extensible than polyelectrolytes of similar molecular weight. In polyelectrolytes, the chains are prestretched by

electrostatic interactions, and the shear viscosity at similar concentration is much higher than of neutral polymers. Thus, the much higher Trouton ratio for neutral polymers is due to higher extensibility as well as much lower shear viscosity value.

Figure 5e shows that the duration of elastocapillary regime and the lifetime of the breakup increase with increasing polyelectrolyte concentration. The extension rate, $\dot{\epsilon} = -2(dR/dt)/R$ values in the inertio-capillary, visco-capillary, and TVC regimes diverge as the pinch-off event is approached, but in the elastocapillary regime, a homogeneous extensional flow with a large, constant, extension rate is established within the neck. The Weissenberg number or the ratio of extension rate to the extensional relaxation rate has a constant value of 2/3 in the elastocapillary regime. The transition from an inertio-capillary regime to elastocapillary regime in the aqueous PAA solutions is relatively sharp, implying that the initial configuration of chains is coil-like in the semidilute solutions, but the high extensional flow field in the neck leads to coil–stretch transition. The resulting pronounced change in macromolecular conformation and the associated increase in drag contribute viscoelastic stresses that compete with capillary stresses, leading to the elastocapillary regime.^{52,53,111,112} For polyelectrolytes in a semidilute solution deformed under comparable extensional rates in cross-slot geometry, birefringence shows a step increase after coil–stretch transition occurs.^{25,30} However, the elastocapillary regime is not observed below overlap concentration (see for example $c = 0.1$ wt % data included in Figure 5e that show primarily the terminal visco-capillary response). The PAA chains are prestretched by electrostatics in dilute solution ($R \propto N^\nu$ expected to show $\nu = 1$). The titration and conductivity measurements indicate that the aqueous PAA solutions used in this study are highly charged, with the charge fraction $f = 1$. Pronounced elastocapillary response is observed for the semidilute, entangled PAA solutions for concentrations above 1 wt %.

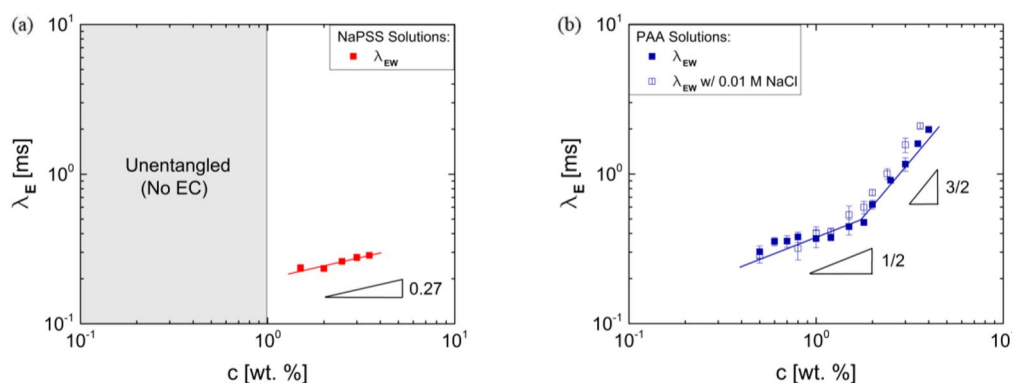


Figure 7. Extensional relaxation time as a function of concentration of the two aqueous polyelectrolyte solutions. (a) The extensional relaxation time as a function of concentration data is measurable only for the nearly entangled aqueous NaPSS solutions. (b) Extensional relaxation time for aqueous PAA solutions is measured for both unentangled and entangled solutions (closed symbols), and additional data was acquired for low salt added (open symbols). Two distinct concentration-dependent scaling regimes are observed with the power law exponents (1/2 and 3/2) that are similar to those observed in the viscosity vs concentration plot for unentangled and entangled semidilute solutions, respectively.

Figures 6a,b show image sequences with 2 ms between each image, and Figure 6c shows a radius evolution plot for a range of aqueous PAA solutions in the semidilute, entangled regime.

As the elastocapillary regime is dominated by a competition between tensile viscoelastic stresses $\eta_E \dot{\epsilon}$ and the capillary stress σ/R , an extensional viscosity measurement can be obtained from the radius evolution data by using the following equation:

$$\eta_E = \frac{\sigma}{\dot{\epsilon}R} = \frac{\sigma}{-2 dR(t)/dt} \quad (4)$$

During the elastocapillary thinning phase, a transient extensional viscosity, $\eta_E^t(\dot{\epsilon}, \epsilon, t)$, is measured using the DoS rheometry technique. Although the extension rate stays constant during the elastocapillary regime, the Hencky strain or the total accumulated strain in the liquid filament, $\epsilon = 2 \ln(R_0/R(t))$, increases steadily, and hence the measured extensional viscosity is plotted as a function of Hencky strain, as shown in Figure 6d. The polyelectrolyte solutions are strain hardening in extension, and the entangled PAA solutions display the Trouton ratio values that are reasonably higher ($10^2 < Tr < 10^3$) than those obtained for the unentangled semidilute aqueous PAA solutions ($Tr < 50$).

Extensional Relaxation Time of Aqueous PAA and NaPSS Solutions. The elastocapillary regime appears linear in a semilog plot of the radius evolution data and can be fit by eq 3 as shown in Figures 5e and 6c. Since the elastocapillary regime for aqueous NaPSS solutions is manifested only for $c > 1$ wt %, the extensional relaxation times are measured only for the semidilute solutions that display $\eta_i \propto c^{0.85}$ (see Figure 2), and the values show very weak concentration dependence of $\lambda_E \propto c^{0.27}$, as shown in Figure 7 (and a table of measured values is included in the Supporting Information). Scaling theories predict that for entangled polyelectrolytes the shear relaxation time remains concentration-independent, and Boris and Colby²⁷ reported that $\lambda \propto c^0$ can be observed for aqueous NaPSS solution (similar molecular weight). However, we checked that the $\lambda \propto c^0$ concentration dependence is only observed for a narrow range of concentrations in the previously reported data sets,^{27,29} and in some cases, like entangled sodium carboxymethyl cellulose solutions,¹⁰¹ a weak concentration dependence is observed.

In contrast, the extensional relaxation times measured for aqueous PAA solutions increase by an order of magnitude (0.2–2 ms) as concentration increases. Furthermore, the PAA

solutions data show that λ_E exhibits a concentration-dependent scaling of $\lambda_E \propto c^{1/2}$ for the unentangled, semidilute regime and $\lambda_E \propto c^{3/2}$ for the entangled regime. The concentration-dependent scaling behavior shown by λ_E data for aqueous PAA solutions in both regimes is strikingly different from the shear relaxation time values predicted by scaling theory and measured experimentally in both the semidilute, unentangled regime^{3,4,26–29,55,99,113} with $\lambda \propto c^{-1/2}$ and the entangled regime with $\lambda \propto c^0$ (independent of concentration).^{2,3,28} Using the intrinsic viscosity of the polyelectrolyte, the Zimm time for the polyelectrolyte chain (in single chain limit) can be estimated using the formula $\lambda = \Lambda[\eta]\eta_s M_w / RT$ (here pre-factor Λ depends on solvent quality and has an $O(1)$ value) which gives $\lambda_Z \approx 0.82$ ms as the estimate for NaPSS and $\lambda_Z \approx 0.15$ ms for PAA solutions. The Zimm time represents a lower bound for relaxation time, and even though the estimated value for PAA solutions is lower, the elastocapillary regime is observed for semidilute, unentangled PAA solutions, and λ_E is measurable for $c > c^*$. In contrast, the unentangled dilute and semidilute aqueous solutions of NaPSS, a strong polyelectrolyte, hence contain chains that are highly prestretched electrostatically, leading to an absence of coil–stretch transition and elastocapillary regime.

The relaxation time values obtained from shear as well as extensional rheology measurements, or from simulations, always increase with concentration for neutral polymers in dilute as well as semidilute solutions.⁵⁹ In the presence of high concentration of salt, the polyelectrolyte solutions are expected to show a weaker concentration-dependent increase (see Table 1). Previous researchers have noted that aqueous solutions with no added salt exposed to air have an effective salt concentration, $c_s \approx 4 \times 10^{-6}$ M, due to dissolved carbon dioxide.^{28,88} However, for the semidilute polyelectrolyte solutions considered here, the effect of dissolved carbon dioxide is expected to be negligible, as the polyelectrolyte concentration is relatively high (or in semidilute solutions, $c_s/c \ll 1$). Furthermore, we verified that the aqueous PAA solutions with a low concentration of added salt ($c_s = 0.01$ M NaCl) exhibit extensional relaxation time values in close agreement with the nominally salt-free solutions. The shear relaxation times for these aqueous polyelectrolyte solutions are not measurable, as the onset of shear thinning lies in a higher shear rate regime, inaccessible in the torsional rheometers. Furthermore, the onset of shear thinning in semidilute

unentangled polyelectrolyte solutions shifts to higher shear rates with an increase in concentration as the relaxation time for polyelectrolytes decreases with concentration.²⁷ In contrast, the onset of shear thinning for neutral polymers shifts to lower shear rates with an increase in concentration, as the longest relaxation time increases steadily with concentration. The shear relaxation time is predicted to remain constant in entangled, semidilute polyelectrolyte solutions. We posited that raising the background solvent viscosity by adding glycerol could provide a simple and effective way of increasing the shear and extensional relaxation time, and thus for reevaluating the concentration-dependent response, as discussed next.

Pinch-Off Dynamics of NaPSS Solutions in Glycerol/Water Mixture Characterized Using DoS Rheometry. Increasing solvent viscosity ($\eta_s = 26.8$ mPa·s) proportionally increases solution shear viscosity and the overall pinch-off time, as apparent from the data sets shown in Figure 8. In contrast to aqueous NaPSS solutions, the capillary thinning dynamics involves evolution as slender cylindrical necks, though the elastocapillary region is again not observed for semidilute unentangled solutions (example montages in Figure 8a,b are for 1 and 3 wt %, both are entangled solutions). Steady shear viscosity of NaPSS solutions in glycerol/water mixture increases with concentration, and as the rate-dependent steady shear viscosity shown in Figure 8d has a well-defined onset of shear thinning, the shear relaxation time can be determined. Following the procedure outlined by Boris and Colby,²⁷ we extracted a shear relaxation time λ_B from the onset of shear thinning by drawing straight line through the rate-dependent viscosity data, and finding its intersection with line drawn through rate-independent viscosity data, as shown in Figure 8d. Alternatively, the rate-dependent viscosity response of the NaPSS solutions can be well described using the Cross model¹¹⁴

$$\eta(\dot{\gamma}) = \eta_\infty + \frac{\eta_0 - \eta_\infty}{1 + (\dot{\gamma}/\dot{\gamma}_c)^m} \quad (5)$$

as shown by the lines in Figure 8d.

The Cross model incorporates four parameters: (i) a rate-independent zero shear viscosity, η_0 ; (ii) an exponent, m , that captures the power law dependence of the viscosity and shear stress on shear rate in the intermediate shear rate region; (iii) a critical strain rate, $\dot{\gamma}_c$ that defines the onset of this power-law region, or alternatively a measure for the shear relaxation time, $\lambda_c = \dot{\gamma}_c^{-1}$; and (iv) a high shear rate viscosity, η_∞ . For these polyelectrolyte solutions, the solvent viscosity was used for the high shear rate viscosity, i.e., $\eta_\infty = \eta_s$, reducing the number of adjustable parameters to three ($\lambda_c = \dot{\gamma}_c^{-1}$, m , and η_0) as summarized in Table 2. Although the generalized Newtonian fluid models¹¹⁵ such as the Cross model cannot predict normal stress phenomena like die swell or any time-dependent viscoelastic effects, such models are useful for computing flow rate and wall shear stresses in steady shear flow conditions and for judging processability over a wide range of shear rates.

The relative viscosity increment data for the NaPSS solutions in glycerol/water mixtures show the concentration dependence $\eta_i \propto c^{1/2}$ expected for unentangled solutions for $c < c_e$ (here $c_e \approx 1$ wt %) and a concentration dependence of $\eta_i \propto c^1$ for entangled solutions, as shown in Figure 9a. The best fits to the entangled solution data (included in the Supporting Information) give $\eta_i \propto c^{1.1}$, and the exponent 1.1 is higher than 0.85 observed for aqueous solution but lower than 3/2

Table 2. Concentration-Dependent Values of Zero Shear Viscosity, Power Law Index, and Shear Relaxation Time as Well as Relaxation Time Value Obtained Using Boris–Colby Fit from Steady Shear Viscosity Data Are Included Together with Extensional Relaxation Time and Apparent Modulus Values Obtained from Fits to Radius Evolution Data for NaPSS Solutions ($M_w = 1000$ kDa) in Glycerol/Water Mixtures (with 70% Glycerol)

c [wt %]	η_0 [Pa·s]	m	λ_c [ms]	λ_B [ms]	λ_E [ms]	G_E [Pa]
1.0	0.20	0.65	1.53	22	3.2	1.46
1.5	0.29	0.64	1.54	22	4.3	1.70
2.0	0.41	0.58	1.79	22	6.2	1.76
2.5	0.52	0.54	2.04	22	7.6	2.21
3.0	0.62	0.58	2.13	22	9.9	2.45

anticipated by the scaling theory. The extensional relaxation time extracted by fitting the radius evolution data with eq 3 (fits shown as dashed line in Figure 8c) shows a concentration-dependent increase of $\lambda_E \propto c^1$ as shown in Figure 9b. In contrast, the shear relaxation time extracted from the onset of shear thinning appears to be concentration-independent in the entire range of concentrations (see λ_B in Figure 9b) if the Boris–Colby protocol is used, or weakly concentration dependent, if the Cross model fit values (λ_c) are compared.

Pinch-Off Dynamics and Extensional Viscosity of PAA Solutions in Glycerol/Water Mixtures. In analogy with the studies carried for NaPSS solutions, here we investigate the shear and extensional rheology response of PAA in glycerol water mixtures, as shown in Figures 10 and 11. In the image sequences included for three PAA solutions (in Figure 10a–c), the cylindrical slender necks characteristic of the viscoelastic response can be observed clearly. The corresponding radius evolution data shown in Figure 10d show a sharper transition into the elastocapillary regime than observed for the NaPSS solutions. The pronounced elastocapillary region is observed for all the concentrations shown in Figure 10d, and the dashed lines show the fit to eq 3. The extensional modulus and extensional relaxation time values extracted from these fits are tabulated in Table 3. The last regime before pinch-off in the radius evolution data for the entangled PAA solutions (see Figure 10d) can be described as the terminal visco-capillary (TVC) regime, implying that the terminal, steady extensional viscosity value is also measured here. The steady shear viscosity data (Figure 10e) show that the onset of shear thinning is clearly manifested for concentrations above 0.5 wt %; however, the onset of shear thinning as determined using the Boris–Colby protocol²⁷ seems to be independent of the concentration. The steady shear viscosity data is also fit using Cross model,¹¹⁴ and the parameters thus obtained are listed in Table 3. Figure 10f shows extensional viscosity as a function of Hencky strain where both apparent extensional stress and Hencky strain are determined using the radius evolution data, using the procedure discussed earlier in this paper. The extensional viscosity values show pronounced concentration-dependent strain hardening as well as the saturation to strain-independent steady, terminal extensional viscosity.

The plot of relative viscosity increment vs concentration shows the two regimes (see Figure 11): the concentration dependence of $\eta_i \propto c^{3/2}$ expected for entangled, semidilute polyelectrolyte solutions is observed for $c > c_e$ (here $c_e \approx 1$ wt %). However, for $c < c_e$ the concentration-dependent variation appears to be stronger than the scaling of $\eta_i \propto c^{1/2}$ expected for

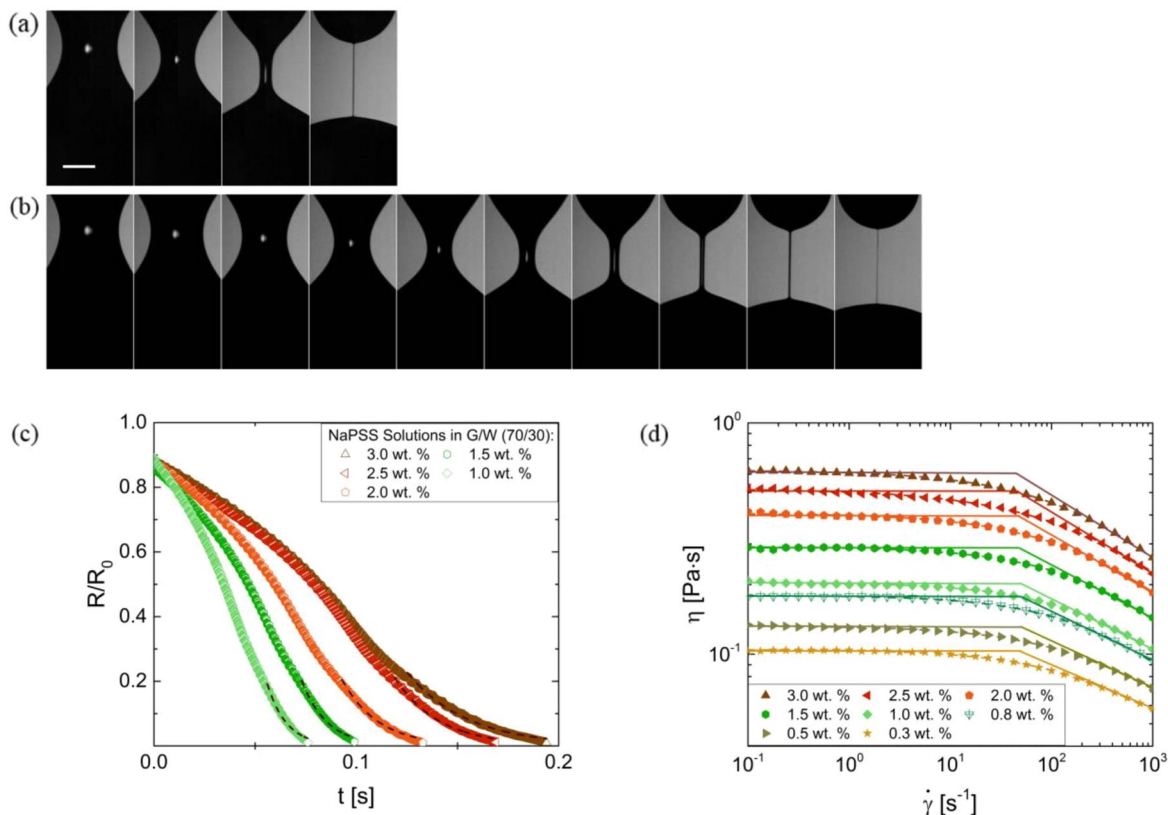


Figure 8. Shear and extensional rheology response for NaPSS solutions in glycerol/water mixtures obtained using torsional rheometry and DoS rheometry respectively. (a, b) Image sequences with time step of 20 ms acquired at 19 000 fps for $c = 1$ and 3 wt % are shown for NaPSS solutions. The neck shape is of a slender filament, characteristic of high-viscosity fluids and of elastic fluids. Scale bar is for 0.5 mm. (c) Radius evolution data plotted on linear–linear axes shows a pronounced elastocapillary response; the fits to eq 3 are shown as a dashed line. (d) Shear viscosity as a function of shear rate shows two regimes: rate-independent regime observed at low shear rates is followed by a shear thinning regime. The straight lines show fits following the Boris–Colby protocol,²⁷ whereas the lines passing through experimental data are the Cross model¹⁴ fits (see text for details).

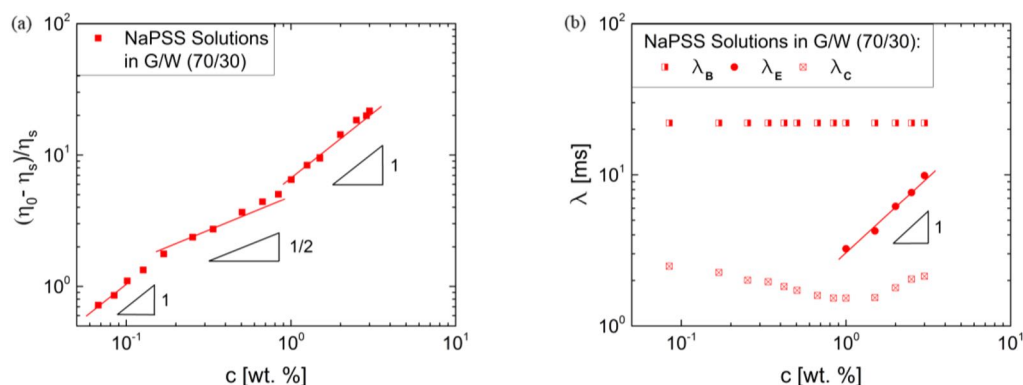


Figure 9. Viscosity and relaxation time measured using shear and extensional rheology of NaPSS solutions in glycerol/water mixture. (a) Relative viscosity increment as a function of concentration for the semidilute NaPSS solutions in glycerol/water mixture increases with $\eta_i \propto c^{1/2}$ in the unentangled and $\eta_i \propto c^1$ in the entangled regime. The transition in scaling in semidilute solution can be identified as the entanglement concentration, $c_e = 1$ wt %. (b) The extensional relaxation time as a function of NaPSS concentration in glycerol/water mixture shows values intermediate to the values of shear relaxation times obtained from shear viscosity data. The two values of shear relaxation time extracted from shear viscosity data are respectively obtained by Boris–Colby fits (λ_B) and the Cross model fits (λ_C); see text for details and Table 2 for values obtained.

semidilute, unentangled polyelectrolyte solutions (the best fit shown in the Supporting Information returns a power law of 0.79). The steady terminal viscosity values obtained for entangled PAA solutions also exhibit a concentration dependence of $\eta_E^\infty \propto c^{3/2}$ (see Supporting Information) mimicking the concentration dependence displayed by the relative viscosity increment measured from the shear rheology response.

Therefore, all solutions show similar $\text{Tr}^\infty = \eta_E^\infty/\eta_0 \approx 350$ value as shown in Figure 11a.

The shear relaxation time data for PAA solutions extracted from the onset of shear thinning determined using Cross model fits of data shown in Figure 10e exhibit two regimes as shown in Figure 11b: in the unentangled regime, $\lambda \propto c^{-1/2}$, which is consistent with the scaling theory predictions and a

Table 3. Concentration-Dependent Values of Zero Shear Viscosity, Power Law Index, and Shear Relaxation Time as Well as Relaxation Time Value Obtained Using the Boris–Colby Fit from Steady Shear Viscosity Data Are Included Together with Extensional Relaxation Time, Apparent Modulus, and Terminal, Steady Extensional Viscosity Values Obtained from Fits to Radius Evolution Data for PAA Solutions ($M_w = 450$ kDa) in Glycerol/Water Mixtures (with 70% Glycerol)

c [wt %]	η_0 [Pa·s]	m	λ_c [ms]	λ_B [ms]	λ_E [ms]	G_E [Pa]	η_E^∞ [Pa·s]
1.0	0.23	0.47	0.9	28	17	43	92
1.5	0.40	0.48	1.2	28	26	119	152
2.0	0.69	0.47	2.2	28	33	34	172
2.5	0.97	0.48	2.6	28	52	79	267
3.0	1.50	0.46	4.5	28	73	248	325

weak increase in the entangled regime. The absolute values of the shear relaxation time obtained using the Boris–Colby procedure are larger in magnitude than the values obtained using the Cross model fit. Furthermore, the Boris–Colby procedure gives a concentration-independent relaxation time, both above and below the entanglement concentration, $c_c \approx 1$ wt %. In contrast, the extensional relaxation times for PAA solutions in glycerol/water mixture show a concentration-

dependent scaling $\lambda_E \propto c^{1/2}$ for the unentangled and $\lambda_E \propto c^{3/2}$ for the entangled regime, consistent with the scaling exponents observed for the aqueous polyelectrolyte solutions. The best fit value for extensional relaxation time data (shown in the Supporting Information) yields an exponent of 0.73, which has a stronger concentration than expected from the scaling theory (and mirrors observations for the relative viscosity increment that yield an exponent of 0.79). The observed concentration-dependent increase of extensional relaxation time for unentangled and entangled semidilute polyelectrolyte solutions, i.e., $\lambda_E \propto c^{1/2}$ and $\lambda_E \propto c^{3/2}$, respectively, has a much weaker concentration dependence than $\lambda_E \propto c^2$ and $\lambda_E \propto c^{14/3}$, respectively, reported for the aqueous solutions of a neutral polymer poly(ethylene oxide) (PEO) in unentangled and entangled regime using CaBER measurements^{116,117} and $\lambda_E \propto c^{3.8}$ reported for entangled solutions of cellulose in an ionic liquid.¹⁰⁹

Influence of Changing Solvent from Water to Glycerol/Water: Discussion. Semidilute aqueous solutions of PAA show the expected concentration dependence $\eta_i \propto c^{1/2}$ for unentangled solutions and $\eta_i \propto c^{3/2}$ for the entangled regime. However, the semidilute solutions of PAA solutions in glycerol/water show a stronger concentration than $\eta_i \propto c^{1/2}$ for unentangled solutions, though $\eta_i \propto c^{3/2}$ is still observed for the entangled regime. Likewise, while NaPSS solutions show the

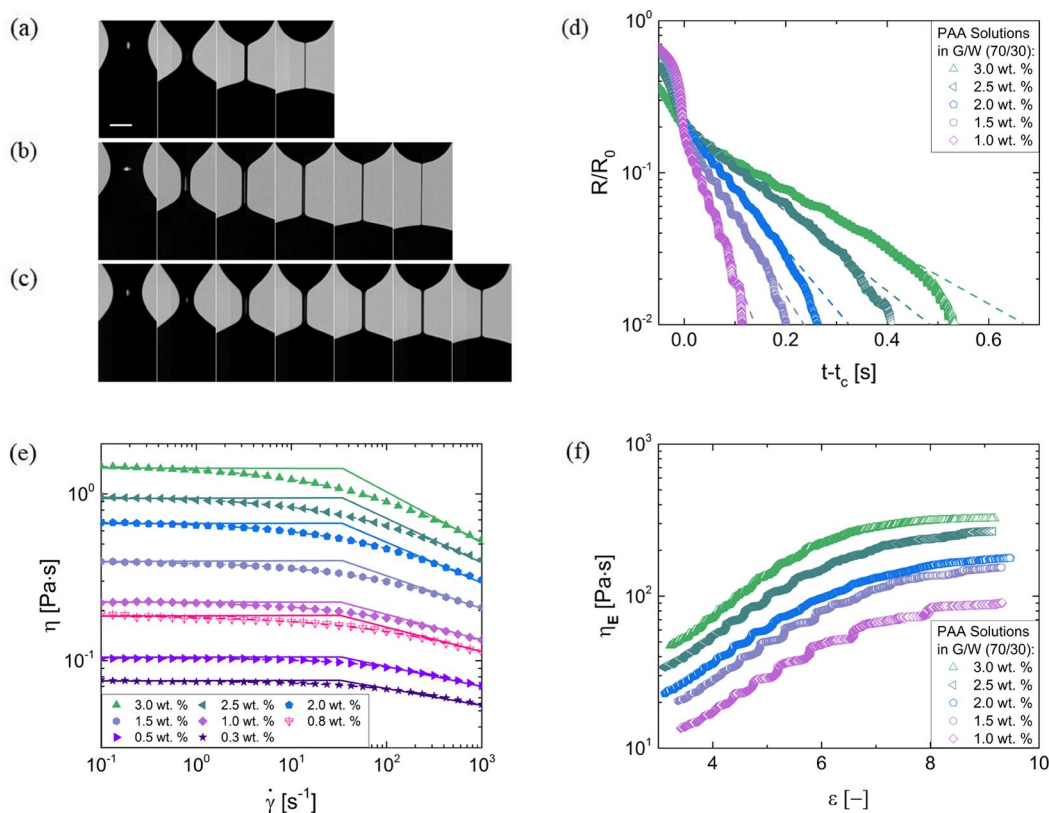


Figure 10. Shear and extensional rheology response of PAA solutions in the glycerol/water mixture. (a–c) Image sequences for PAA solutions with time step of 60 ms, acquired at 19 000 fps, for $c = 1, 2,$ and 2.5 wt %. Scale bar is for 0.5 mm. (d) Radius evolution plot for PAA solutions with the x -axis shifted to show an overlapping t_c . The dashed lines show the fits to the elastocapillary regime obtained by using eq 3. (e) Shear viscosity as a function of shear rate shows two regimes: rate-independent regime observed at low shear rates is followed by a shear thinning regime. The straight lines show fits following the Boris–Colby protocol²⁷ (see text), whereas the lines passing through experimental data (symbols) are the Cross model¹¹⁴ fits. (f) Extensional viscosity as a function of Hencky strain, obtained by analyzing the radius evolution data shown in (d). The extensional viscosity increases with strain and strain rate, showing strain hardening in contrast to shear thinning behavior manifested in the steady shear viscosity measurements.

expected concentration dependence $\eta_i \propto c^{1/2}$ for unentangled solutions in both solvents, entangled solutions in water exhibit $\eta_i \propto c^{0.85}$ and a stronger $\eta_i \propto c^{1.1}$ dependence in glycerol/water mixture (see best fits to data, included in the [Supporting Information](#)). Likewise, the extensional relaxation time values for unentangled PAA solutions and entangled NaPSS solutions display stronger concentration-dependent increase in glycerol–water solutions. Changing the solvent from water to glycerol/water mixture results in (a) 30-fold increase in solvent viscosity, (b) decrease in dielectric constant by 68%, (c) increase in density by a factor of 1.19, (d) change in solvent quality and solvent–polymer interactions (influences excluded volume interactions, hydrogen bonding, and hydrophobicity), and (e) decrease in surface tension. The change in solvent–polymer interactions and change in dielectric constant influence the observed changes in exponents that capture the concentration-dependent shear and extensional response. Next we discuss how the cumulative influence of increase in solvent viscosity and decrease in solvent quality and dielectric constant affect shear viscosity and intrinsic viscosity of the two polyelectrolytes.

A comparison of shear viscosity of 0.5% PAA solution in water and in glycerol/water mixture shows that even though solvent viscosity is increased by 26 times, the solution viscosity increases only by a factor of 5, and likewise for 0.5% NaPSS solutions, the shear viscosity increases by less than 3 times. Since the solution viscosity is exactly twice the solvent viscosity at $c^* = 0.1$ wt % for NaPSS solution and $c^* = 0.2$ wt % PAA in glycerol–water mixture, the intrinsic viscosity estimates respectively are $[\eta]^{\text{NaPSS}} \approx 10$ dL/g and $[\eta]^{\text{PAA}} \approx 5$ dL/g, in contrast to aqueous solutions that display $[\eta]^{\text{NaPSS}} \approx 50$ dL/g and $[\eta]^{\text{PAA}} \approx 20$ dL/g, respectively. The decrease in intrinsic viscosity implies that the pervaded volume is smaller, and thus polyelectrolyte chains are less expanded in the glycerol/water mixture. Thus, the increase in solvent viscosity by 26 times is offset by a 4- and 5-fold decrease in pervaded volume (at overlap concentration) of PAA and NaPSS, respectively. Likewise, the shear relaxation time can be contrasted in two solvents, but as shear relaxation time values are not measured in our experiments with aqueous solutions, we estimate and contrast the Zimm time (for the polyelectrolyte chain in single chain limit) using the formula $\lambda_z = \Lambda[\eta]\eta_s M_w / RT$. As Zimm time depends on both intrinsic viscosity and solvent viscosity, we find $\lambda_z \approx 4.9$ ms as the estimate for NaPSS and $\lambda_z \approx 1.3$ ms for PAA solutions, in contrast to $\lambda_z \approx 0.82$ ms and $\lambda_z \approx 0.15$ ms for the corresponding aqueous solutions. The experimental results for the overall pinch-off time as well as the measured relaxation times of the semidilute polyelectrolyte solutions also show that the effect of increase in solvent viscosity is offset to some extent by a decrease in the pervaded volume of the polyelectrolyte chains.

Extensional Relaxation Time of Polyelectrolyte Solutions: Discussion. Although there are no previous comprehensive studies of concentration-dependent extensional relaxation times for polyelectrolyte solutions, for neutral polymers including aqueous solutions of poly(ethylene oxide), experimental data from Dinic et al.⁵³ show two distinct regimes: the concentration-dependent scaling $\lambda_E \sim c^m$ has exponent $m \approx 0.65$ for dilute solutions ($c/c^* < 1$), whereas $m \approx 1$ for intrinsically semidilute, unentangled solutions ($1 < c/c^* < c_c/c^*$; intrinsically emphasizes that even unperturbed coils are interpenetrating and interacting with each other). Furthermore, for dilute solutions of neutral polymers, the

extensional relaxation time measured is often larger in magnitude than the value of relaxation time obtained in oscillatory shear or stress relaxation experiments;^{19,25,40,71–76} however, in the semidilute solutions both relaxation times show a comparable magnitude. Following the arguments of de Gennes,^{51,56} Pincus,^{118,119} and Brochard-Wyatt et al.²⁵ that outline relaxation dynamics for single stretched chains using tension blob concepts, Dinic et al.⁵³ argued that in extensional flows the stretching of polymer coils leads to progressive screening of excluded volume (EV) interactions as well as change in the local hydrodynamic interactions due to conformational anisotropy, leading to increased screening of the EV interactions. For PEO solutions with $c < c^*$, through the unperturbed coils do not interpenetrate, the intrachain and interchain interactions dramatically change as the chain gets progressively stretched by extensional flow, and many groups have argued that the stretched chain hydrodynamics could be described using blob models used for semidilute solutions.^{40,52,77,120–122} However, the concentration-dependent scaling observed in experiments changes dramatically above overlap concentration, and therefore the solutions for $c > c^*$ were designated as the intrinsically semidilute solutions. The stretched PEO Rouse–Zimm chains in intrinsically semidilute solutions show scaling law obtained in blob models for theta solvent even though water is a good solvent for PEO.⁵³ Due to electrostatic stretching of chains and the presence of electrostatic interactions, the theoretical description of dynamics of semidilute polyelectrolytes is more challenging, even more so, when the chains are additionally stretched by flow.

We postulate that the polyelectrolyte chain conformations in both dilute and semidilute solutions can display one of the following two types of transitions with increasing extensional rate. Type I behavior could arise for polyelectrolytes with higher flexibility (determined by both intrinsic and electrostatic persistence length^{1–4}) and larger extensibility (defined as ratio of the size of fully stretched chain to its equilibrium size). First, a coil–stretch transition can transform a swollen coil made up of correlation blobs into a stretched chain of tension blobs (the tension blobs could be smaller than the correlation blobs and larger than the electrostatic), and a second transition could occur to the nearly fully extended chain. Type II behavior would arise for lower concentration solutions, and also for polyelectrolytes with lower extensibility and lower flexibility, such that even at the quiescent state the chain conformation is akin to a prestretched chain of electrostatic blobs, and the only possibility is a transition to a nearly fully extended state. In the present study, aqueous NaPSS solutions in unentangled, semidilute solutions display the type II behavior, and hence elastocapillary response that arises in unentangled solutions due to coil–stretch transition is not observed. In contrast, the presence of a pronounced elastocapillary regime that appears after a sharp change from initial inertio-capillary thinning response suggests that PAA macromolecules in unentangled, semidilute solution undergo the coil–stretch transition. In this case, under the influence of sustained extensional strain, the prestretched chains of tension blobs transition to fully extended chains which leads to the terminal visco-capillary (TVC) regime, observed in the radius evolution data sets for semidilute, unentangled PAA solutions. The concentration-dependent relaxation dynamics of polyelectrolyte chains that have undergone both hydrodynamic and

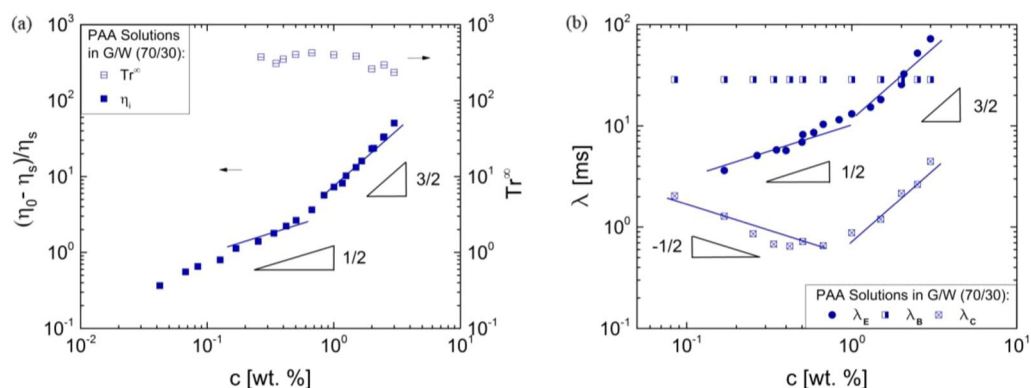


Figure 11. Viscosity and relaxation time measured using shear and extensional rheology for PAA solutions in glycerol/water mixtures. (a) Relative viscosity increment plotted as a function of PAA concentration is shown in closed symbols, and the terminal Trouton ratio, estimated from the ratio of steady, terminal extensional viscosity and zero shear viscosity, is shown in open symbols. (b) Extensional relaxation time as a function of PAA concentration in glycerol/water mixture (closed symbols) shows two distinct scaling exponents of 1/2 and 3/2 for the unentangled and entangled solutions, respectively. The two shear relaxation times values extracted from shear viscosity data are obtained by the Boris–Colby²⁷ protocol and the Cross model¹¹⁴ fits.

electrostatic stretching can be derived using this phenomenological picture, as discussed next.

In the tension blob description of a stretched chain, the Pincus relation $F = kT/\xi_t$ sets the length scale for local interactions. In the 1970s, Pincus postulated that single polymer chains under tension (force, F) can be described by considering an equivalent chain made up of tension blobs^{56,118,119} (or Pincus blobs), such that structural anisotropy and the influence of the applied tension on intrachain interactions play a role only above ξ_t . However, the macromolecular level description of dynamics of a stretched chain surrounded by a sea of similarly stretched chains in a good solvent is still lacking in the literature. Following ideas put forth in the context of drag on a tethered chain moving in sea of other chains¹²³ and the effective medium theory to describe hydrodynamics of unentangled chains,¹²⁴ we provide a mean-field model for semidilute polyelectrolyte solutions by arguing that the drag experienced by each tension blob is proportional to the solution viscosity, rather than the solvent viscosity. We postulate that beyond a critical extensional rate that satisfies $\dot{\epsilon}_c \lambda_E \sim 1$, the stretched chains must be described as a string of tension blobs rather than as a chain of correlation blobs. Every blob in the stretched chain experiences a drag force $F_{d0} = \eta_p \xi_t V$, such that for $\dot{\epsilon}_c \sim V/\xi_t$ and for N/g_t tension blobs the following expressions can be deduced for the unentangled polyelectrolyte solutions:

$$F \approx \frac{N}{g} \eta_p \xi_t^2 \dot{\epsilon}_c = \frac{kT}{\xi_t} \quad (6a)$$

$$\lambda_E \approx \frac{N}{g_t} \frac{\eta_p \xi_t^3}{kT} \approx N \frac{\eta_p b^3}{kT} g_t^{1/2} \quad (6b)$$

For a chain that has undergone both hydrodynamic and electrostatic stretching, the number of bonds in a tension blob should be a small number (implying $g_t^{1/2} \approx O(1)$). Though the scaling argument and the expressions capture the concentration-dependent scaling observed for the four semidilute unentangled solutions considered in this study, a more robust model is needed to account for the influence of both interchain and intrachain interactions and the interplay of hydrodynamic and electrostatic stretching, as well for evaluating the effective medium viscosity for a dispersion of stretched polymers. For

the entangled polyelectrolyte solutions, deriving an expression for the extensional relaxation time would require a careful assessment of entanglements, as well as of both electrostatic and elasticity effects, and is left as a problem for a future investigation. Even though the extensional relaxation time and relative viscosity increment exhibit similar exponent for the concentration-dependent behavior for the entangled PAA solutions in both solvents and entangled NaPSS solutions in glycerol/water mixture, any deduction for relaxation time for the entangled chains requires an assessment of the number and dynamics of topological constraints.

Printability, Spinnability, and Jettability of Aqueous Polyelectrolyte Solutions. Polyelectrolytes are used as rheology modifiers in many applications and are present in many biologically relevant fluids. Addition of a much lower concentration of polyelectrolytes is required to provide the same enhancement in shear viscosity as obtained with neutral polymers, and decreasing the amount of rheological modifier provides savings in terms of material costs. The dripping-onto-substrate rheometry characterization shows that the extensional relaxation time and pinch-off times for the polyelectrolytes are relatively short, and addition of polyelectrolytes suppresses satellite drop formation. Shorter pinch-off times allow faster processing speeds. Because of the electrostatic prestretching of chains, strong polyelectrolytes exist in their extended conformation, and in the absence of a coil–stretch transition, the elastocapillary regime is not realized in the radius evolution data sets for strong polyelectrolytes below entanglement concentration. In the entangled semidilute solutions, however, a hint of elastocapillary regime can be observed, but the capillary-driven thinning and pinch-off are relatively short, and although this is ideal for drop formation applications, filament spinning would be challenging in comparison with flexible neutral polymer solutions. However, if desired, fibers can be spun using strong polyelectrolytes by adding a small amount of high molecular weight flexible neutral polymer like poly(ethylene oxide).^{125,126} The weak polyelectrolytes show the elastocapillary regime for both entangled and unentangled semidilute solutions, but due to lower flexibility and extensibility, pinch-off occurs in a relatively short time compared to neutral flexible polymers like poly(ethylene oxide).

CONCLUSIONS

In the present contribution, we contrast the shear and extensional response of aqueous solutions of two representative polyelectrolytes—poly(sodium 4-styrenesulfonate) (NaPSS) and poly(acrylic acid) (PAA)—in the absence of added salts in two solvents: water and a higher viscosity water–glycerol mixture. The steady shear viscosity measurements with aqueous polyelectrolyte solutions show nearly rate-independent values that increase with concentration of the added polymer. The intrinsic viscosity values estimated using $c^*[\eta] \approx 1$ for the aqueous NaPSS and PAA solutions are $[\eta]^{\text{NaPSS}} \approx 50$ dL/g and $[\eta]^{\text{PAA}} \approx 20$ dL/g, respectively, and in the glycerol/water (70:30) mixture, the intrinsic viscosity values decrease to $[\eta]^{\text{NaPSS}} \approx 10$ dL/g and $[\eta]^{\text{PAA}} \approx 5$ dL/g, respectively. In contrast, the intrinsic viscosity value for aqueous PEO solution (neutral polymer in good solvent, with $M_w = 1000$ kDa) is 6 dL/g. The higher intrinsic viscosity values of aqueous NaPSS solutions ($M_w = 1000$ kDa) as well as of aqueous PAA solutions ($M_w = 450$ kDa) show that the polyelectrolyte chains are stretched electrostatically compared to a neutral polymer and that changing solvent–polymer interactions influences equilibrium coil size of polyelectrolytes. Semidilute PAA solutions in water show the expected concentration dependence $\eta_i \propto c^{1/2}$ for unentangled solutions and $\eta_i \propto c^{3/2}$ for the entangled regime. However, the semidilute solutions of PAA in glycerol/water mixture show stronger concentration than $\eta_i \propto c^{1/2}$ for unentangled solutions, though $\eta_i \propto c^{3/2}$ is still observed for the entangled regime. The steady, terminal extensional viscosity measurements for entangled, semidilute PAA solutions in glycerol/water mixture also exhibit the same concentration dependence of $\eta_E^\infty \propto c^{3/2}$ leading to a nearly constant value of terminal Trouton ratio, $\text{Tr}^\infty = \eta_E^\infty/\eta_0 \approx 350$. However, even though the aqueous NaPSS solutions show the expected concentration-dependent behavior for the semidilute unentangled regime, $\eta_i \propto c^{1/2}$, a concentration dependence with $\eta_i \propto c^{0.85}$ is observed at higher concentrations of $c > 1$ wt % ($20c^*$). The power law scaling of $\eta_i \propto c^{1/2}$ is characteristic of polyelectrolyte solutions for the neutral polymers do not display any regime with $\eta_i \propto c^{1/2}$, and for $c > c^*$, a stronger concentration dependence $\eta_i \propto c^{1.3}$ is observed for semidilute, unentangled solutions of neutral polymers.⁵⁵

The extensional relaxation times, λ_E , are not measurable for aqueous NaPSS in the semidilute, unentangled regime but exhibit a relatively weak increase with concentration in the entangled regime. However, for NaPSS solutions in the glycerol/water mixture, the λ_E values measured in the semidilute, entangled solutions increase linearly with concentration. In contrast, the measured λ_E for semidilute solutions of PAA in water as well as in glycerol/water mixture exhibits a concentration-dependent scaling of $\lambda_E \propto c^{1/2}$ for the unentangled (the best fit values of PAA in G/W mixture yield an exponent of 0.73) and $\lambda_E \propto c^{3/2}$ for the entangled regime. The concentration-dependent scaling behavior shown by λ_E data for PAA solutions in both regimes is strikingly different from the predicted exponents for shear relaxation time of semidilute polyelectrolyte solutions in both the unentangled regime ($\lambda \propto c^{-1/2}$) and the entangled regime ($\lambda \propto c^0$; independent of concentration). Though aqueous solutions of both polyelectrolytes display a nearly rate-independent steady shear viscosity, the solutions made in higher viscosity glycerol/water mixtures can be used for estimating the shear relaxation time, λ . The extracted values of

λ obtained from the onset of shear thinning determined using Boris–Colby fits of steady shear viscosity data appears to be concentration-independent for both NaPSS and PAA. The shear relaxation time data for PAA solutions in glycerol–water mixture extracted from the onset of shear thinning determined using Cross model fits of data shows $\lambda \propto c^{-1/2}$ in the unentangled regime, consistent with scaling theories and a weak increase in the entangled regime (scaling theories predict $\lambda \propto c^0$). In contrast, the extensional relaxation times for PAA solutions in glycerol/water mixture show concentration-dependent scaling $\lambda_E \propto c^{1/2}$ for the unentangled and $\lambda_E \propto c^{3/2}$ for the entangled regime, consistent with the scaling observed for the aqueous PAA solutions. The increase in extensional relaxation time for polyelectrolyte solutions in the semidilute unentangled as well as entangled regime is thus a self-consistent feature of multiple measurements. We have verified similar increase in extensional relaxation time also occurs for several different molecular weights of hydrolyzed polyacrylamide (HPAM), and the data sets will be described in another study. Increased degree of interchain overlap, increase in the screening of both excluded volume interactions and hydrodynamic interactions, and possibly increased screening of electrostatic interactions all combine together to provide the concentration-dependent values for extensional relaxation time for polyelectrolyte solutions.

We provide a phenomenological scaling argument that captures the concentration-dependent behavior shown by the extensional relaxation time of polyelectrolyte chains in unentangled, semidilute polyelectrolyte solutions. We argue that the observed relaxation dynamics can be described by recognizing that hydrodynamically stretched chains can be considered to be a string of tension blobs (rather than correlation blobs), and for such stretched chains, the drag coefficient for each blob is effectively proportional to solution viscosity (invoking a coarse-grained, effective medium description). The experimental data sets included here highlight the fact that polyelectrolytes provide a greater enhancement in shear viscosity for relatively low weight fraction, but for similar molecular weight, polyelectrolytes possess lower flexibility and lower extensibility than neutral polymers, leading to a lower degree of strain hardening and shorter relaxation time and pinch-off time and, thus, increased suitability as rheology modifiers for printability applications. As many formulations contain additives that can affect the electrostatic interactions, a careful study of, say, the effect of salt on extensional relaxation times, pinch-off dynamics, and shear rheology response is needed and is underway.

ASSOCIATED CONTENT

Supporting Information

The Supporting Information is available free of charge on the ACS Publications website at DOI: 10.1021/acs.macromol.8b00148.

Figures S1–S5 and Table S1 (PDF)

Movie S1 (AVI)

Movie S2 (AVI)

Movie S3 (AVI)

Movie S4 (AVI)

Movie S5 (AVI)

Movie S6 (AVI)

Movie S7 (AVI)

■ AUTHOR INFORMATION

Corresponding Author

*(V.S.) E-mail: viveks@uic.edu.

ORCID 

Vivek Sharma: 0000-0003-1152-1285

Notes

The authors declare no competing financial interest.

■ ACKNOWLEDGMENTS

V.S. acknowledges funding support by the College of Engineering and the Department of Chemical Engineering at the University of Illinois at Chicago. The students (J.D. and L.N.J.) were supported by the start-up funds as well as funding by the Campus Research Board (CRB). L.N.J. also acknowledges sustained funding (Teaching Assistantship) by the Department of Chemistry at UIC. V.S. thanks Prof. Samanvaya Srivasatava for close reading of the manuscript and Prof. Tim Lodge for suggesting a comparison between aqueous solutions of PAA prepared without salt and with low concentration of added salt.

■ REFERENCES

- (1) Muthukumar, M. *50th Anniversary Perspective: A perspective on polyelectrolyte solutions*. *Macromolecules* **2017**, *50* (24), 9528–9560.
- (2) Muthukumar, M. Dynamics of polyelectrolyte solutions. *J. Chem. Phys.* **1997**, *107* (7), 2619–2635.
- (3) Dobrynin, A. V. Solutions of charged polymers. *Polymer Science: A Comprehensive Reference* **2012**, *1*, 81–132.
- (4) Dobrynin, A. V.; Rubinstein, M. Theory of polyelectrolytes in solutions and at surfaces. *Prog. Polym. Sci.* **2005**, *30* (11), 1049–1118.
- (5) Holm, C.; Joanny, J. F.; Kremer, K.; Netz, R. R.; Reineker, P.; Seidel, C.; Vilgis, T. A.; Winkler, R. G. Polyelectrolyte theory. In *Polyelectrolytes with Defined Molecular Architecture II*; Springer: 2004; pp 67–111.
- (6) Netz, R. R.; Andelman, D. Neutral and charged polymers at interfaces. *Phys. Rep.* **2003**, *380* (1), 1–95.
- (7) Barrat, J.-L.; Joanny, J.-F. Theory of polyelectrolyte solutions. *Adv. Chem. Phys.* **1997**, *1*.
- (8) Wong, G. C. L.; Pollack, L. Electrostatics of strongly charged biological polymers: ion-mediated interactions and self-organization in nucleic acids and proteins. *Annu. Rev. Phys. Chem.* **2010**, *61*, 171–189.
- (9) Radeva, T. *Physical Chemistry of Polyelectrolytes*; CRC Press: 2001; Vol. 99.
- (10) Williams, P. A. *Handbook of Industrial and Water Soluble Polymers*; Blackwell Publishing Ltd.: Oxford, 2007.
- (11) Calvert, P. Inkjet printing for materials and devices. *Chem. Mater.* **2001**, *13* (10), 3299–3305.
- (12) Derby, B. Bioprinting: inkjet printing proteins and hybrid cell-containing materials and structures. *J. Mater. Chem.* **2008**, *18* (47), 5717–5721.
- (13) Kumar, S. Liquid transfer in printing processes: liquid bridges with moving contact lines. *Annu. Rev. Fluid Mech.* **2015**, *47* (1), 67–94.
- (14) Eggers, J. Nonlinear dynamics and breakup of free-surface flows. *Rev. Mod. Phys.* **1997**, *69* (3), 865–929.
- (15) Eggers, J.; Villermaux, E. Physics of liquid jets. *Rep. Prog. Phys.* **2008**, *71* (3), 036601.
- (16) Ashgriz, N. *Handbook of Atomization and Sprays: Theory and Applications*; Springer: New York, 2011.
- (17) Middleman, S. *Modeling Axisymmetric Flows: Dynamics of Films, Jets and Drops*; Academic Press: San Diego, 1995.
- (18) Basaran, O. A. Small-scale free surface flows with breakup: Drop formation and emerging applications. *AIChE J.* **2002**, *48* (9), 1842–1848.
- (19) McKinley, G. H. Visco-elastocapillary thinning and break-up of complex fluids. *Rheol. Rev.* **2005**, 1–48.
- (20) Schummer, P.; Tebel, K. H. A new elongational rheometer for polymer solutions. *J. Non-Newtonian Fluid Mech.* **1983**, *12* (3), 331–347.
- (21) Schummer, P.; Tebel, K. H. Design and operation of the free jet elongational rheometer. *Rheol. Acta* **1982**, *21* (4–5), 514–516.
- (22) Ardekani, A.; Sharma, V.; McKinley, G. H. Dynamics of bead formation, filament thinning and breakup of weakly viscoelastic jets. *J. Fluid Mech.* **2010**, *665*, 46–56.
- (23) Sharma, V.; Haward, S. J.; Serdy, J.; Keshavarz, B.; Soderlund, A.; Threlfall-Holmes, P.; McKinley, G. H. The rheology of aqueous solutions of Ethyl Hydroxy-Ethyl Cellulose (EHEC) and its hydrophobically modified Analogue (hmEHEC): Extensional flow response in capillary break-up, jetting (ROJER) and in a cross-slot extensional rheometer. *Soft Matter* **2015**, *11* (16), 3251–3270.
- (24) Keshavarz, B.; Sharma, V.; Houze, E. C.; Koerner, M. R.; Moore, J. R.; Cotts, P. M.; Threlfall-Holmes, P.; McKinley, G. H. Studying the Effects of Elongational Properties on Atomization of Weakly Viscoelastic Solutions Using Rayleigh Ohnesorge Jetting Extensional Rheometry (ROJER). *J. Non-Newtonian Fluid Mech.* **2015**, *222*, 171–189.
- (25) Nguyen, T. Q.; Kausch, H. H. *Flexible Polymer Chains in Elongational Flow: Theory and Experiment*; Springer-Verlag: Berlin, 1999.
- (26) Colby, R. H. Structure and linear viscoelasticity of flexible polymer solutions: comparison of polyelectrolyte and neutral polymer solutions. *Rheol. Acta* **2010**, *49* (5), 425–442.
- (27) Boris, D. C.; Colby, R. H. Rheology of sulfonated polystyrene solutions. *Macromolecules* **1998**, *31* (17), 5746–5755.
- (28) Dobrynin, A. V.; Colby, R. H.; Rubinstein, M. Scaling theory of polyelectrolyte solutions. *Macromolecules* **1995**, *28* (6), 1859–1871.
- (29) Dou, S.; Colby, R. H. Solution rheology of a strongly charged polyelectrolyte in good solvent. *Macromolecules* **2008**, *41* (17), 6505–6510.
- (30) Miles, M. J.; Tanaka, K.; Keller, A. The behavior of polyelectrolytes in elongational flow; the determination of conformational relaxation times (with an Appendix of an anomalous adsorption effect). *Polymer* **1983**, *24* (9), 1081–1088.
- (31) Narh, K. A.; Odell, J. A.; Keller, A. Temperature dependence of the conformational relaxation time of polymer molecules in elongational flow; invariance of the molecular weight exponent. *J. Polym. Sci., Part B: Polym. Phys.* **1992**, *30* (4), 335–340.
- (32) Narh, K. A.; Keller, A. The effect of counterions on the chain conformation of polyelectrolytes, as assessed by extensibility in elongational flow: The influence of multiple valency. *J. Polym. Sci., Part B: Polym. Phys.* **1994**, *32* (10), 1697–1706.
- (33) Carrington, S.; Odell, J.; Fisher, L.; Mitchell, J.; Hartley, L. Polyelectrolyte behaviour of dilute xanthan solutions: Salt effects on extensional rheology. *Polymer* **1996**, *37* (13), 2871–2875.
- (34) Dunlap, P. N.; Leal, L. G. The charged dumbbell model for dilute polyelectrolyte solutions in strong flows. *Rheol. Acta* **1984**, *23* (3), 238–249.
- (35) Dunlap, P. N.; Wang, C. H.; Leal, L. G. An experimental study of dilute polyelectrolyte solutions in strong flows. *J. Polym. Sci., Part B: Polym. Phys.* **1987**, *25* (11), 2211–2238.
- (36) Borisov, O. V.; Darinskii, A. A.; Zhulina, E. B. Stretching of polyelectrolyte coils and globules in an elongational flow. *Macromolecules* **1995**, *28* (21), 7180–7187.
- (37) Darinskii, A. A.; Borisov, O. V. Polyelectrolyte molecule in an elongational flow. *Europhys. Lett.* **1995**, *29* (5), 365–370.
- (38) Funatsu, Y.; Fukao, K.; Miyamoto, Y. Elongational flow study of poly(styrene sulfonate) in dilute solution. *Polymer* **1997**, *38* (11), 2857–2860.
- (39) Liu, S.; Ashok, B.; Muthukumar, M. Brownian dynamics simulations of bead-rod-chain in simple shear flow and elongational flow. *Polymer* **2004**, *45* (4), 1383–1389.

- (40) Stelter, M.; Brenn, G.; Yarin, A. L.; Singh, R. P.; Durst, F. Validation and application of a novel elongational device for polymer solutions. *J. Rheol.* **2000**, *44* (3), 595–616.
- (41) Andrews, N. C.; McHugh, A. J.; Schieber, J. D. Polyelectrolytes in shear and extensional flows: Conformation and rheology. *J. Polym. Sci., Part B: Polym. Phys.* **1998**, *36* (8), 1401–1417.
- (42) Jiang, L.; Chen, S. B. Electroviscous effect on the rheology of a dilute solution of flexible polyelectrolytes in extensional flow. *J. Non-Newtonian Fluid Mech.* **2001**, *96* (3), 445–458.
- (43) Pamies, R.; Cifre, J. G. H.; De la Torre, J. G. Brownian dynamics simulation of polyelectrolyte dilute solutions: Relaxation time and elongational flow. *J. Polym. Sci., Part B: Polym. Phys.* **2007**, *45* (6), 714–722.
- (44) Sasaki, N.; Ashitaka, H.; Ohtomo, K.; Fukui, A. Hydrodynamic properties of DNA and DNA-lipid complex in an elongational flow field. *Int. J. Biol. Macromol.* **2007**, *40* (4), 327–335.
- (45) Stoltz, C.; de Pablo, J. J.; Graham, M. D. Concentration dependence of shear and extensional rheology of polymer solutions: Brownian dynamics simulations. *J. Rheol.* **2006**, *50* (2), 137–167.
- (46) Larson, R. G. The rheology of dilute solutions of flexible polymers: Progress and problems. *J. Rheol.* **2005**, *49* (1), 1–70.
- (47) Schroeder, C. M.; Babcock, H. P.; Shaqfeh, E. S. G.; Chu, S. Observation of polymer conformation hysteresis in extensional flow. *Science* **2003**, *301* (5639), 1515–1519.
- (48) Schroeder, C. M.; Shaqfeh, E. S. G.; Chu, S. Effect of hydrodynamic interactions on DNA dynamics in extensional flow: Simulation and single molecule experiment. *Macromolecules* **2004**, *37* (24), 9242–9256.
- (49) Schroeder, C. M. Single polymer dynamics for molecular rheology. *J. Rheol.* **2018**, *62* (1), 371–403.
- (50) Hinch, E. J. Uncoiling a polymer molecule in a strong extensional flow. *J. Non-Newtonian Fluid Mech.* **1994**, *54*, 209–230.
- (51) de Gennes, P. G. Coil-stretch transition of dilute flexible polymers under ultrahigh velocity gradients. *J. Chem. Phys.* **1974**, *60* (12), 5030–5042.
- (52) Dinic, J.; Zhang, Y.; Jimenez, L. N.; Sharma, V. Extensional Relaxation Times of Dilute, Aqueous Polymer Solutions. *ACS Macro Lett.* **2015**, *4* (7), 804–808.
- (53) Dinic, J.; Biagioli, M.; Sharma, V. Pinch-off dynamics and extensional relaxation times of intrinsically semi-dilute polymer solutions characterized by dripping-onto-substrate rheometry. *J. Polym. Sci., Part B: Polym. Phys.* **2017**, *55* (22), 1692–1704.
- (54) Dinic, J.; Jimenez, L. N.; Sharma, V. Pinch-off dynamics and dripping-onto-substrate (DoS) rheometry of complex fluids. *Lab Chip* **2017**, *17*, 460–473.
- (55) Rubinstein, M.; Colby, R. H. *Polymer Physics*; Oxford University Press: New York, 2003.
- (56) de Gennes, P.-G. *Scaling Concepts in Polymer Physics*; Cornell University Press: Ithaca, NY, 1979.
- (57) Muthukumar, M. Polyelectrolyte dynamics. *Adv. Chem. Phys.* **2005**, *131*, 1–60.
- (58) Zimm, B. H. Dynamics of polymer molecules in dilute solution: viscoelasticity, flow birefringence and dielectric loss. *J. Chem. Phys.* **1956**, *24*, 269–278.
- (59) Doi, M.; Edwards, S. F. *The Theory of Polymer Dynamics*; Oxford University Press: New York, 1986; p 406.
- (60) Rouse, P. E., Jr. A theory of the linear viscoelastic properties of dilute solutions of coiling polymers. *J. Chem. Phys.* **1953**, *21* (7), 1272–1280.
- (61) Eom, S. H.; Senthilarasu, S.; Uthirakumar, P.; Yoon, S. C.; Lim, J.; Lee, C.; Lim, H. S.; Lee, J.; Lee, S.-H. Polymer solar cells based on inkjet-printed PEDOT: PSS layer. *Org. Electron.* **2009**, *10* (3), 536–542.
- (62) Novák, P.; Müller, K.; Santhanam, K.; Haas, O. Electrochemically active polymers for rechargeable batteries. *Chem. Rev.* **1997**, *97* (1), 207–282.
- (63) Christensen, N. D.; Reed, C. A.; Culp, T. D.; Hermonat, P. L.; Howett, M. K.; Anderson, R. A.; Zaneveld, L. J. Papillomavirus microbicidal activities of high-molecular-weight cellulose sulfate, dextran sulfate, and polystyrene sulfonate. *Antimicrob. Agents Chemother.* **2001**, *45* (12), 3427–3432.
- (64) Wever, D. A. Z.; Picchioni, F.; Broekhuis, A. A. Polymers for enhanced oil recovery: A paradigm for structure-property relationship in aqueous solution. *Prog. Polym. Sci.* **2011**, *36* (11), 1558–1628.
- (65) Laba, D. *Rheological Properties of Cosmetics and Toiletries*; Marcel Dekker, Inc.: New York, 1993.
- (66) Staudinger, H.; Urech, E. Über hochpolymere Verbindungen. 31. Mitteilung. Über die Poly-acrylsäure und Poly-acrylsäure-ester. *Helv. Chim. Acta* **1929**, *12* (1), 1107–1133.
- (67) Markovitz, H.; Kimball, G. E. The effect of salts on the viscosity of solutions of polyacrylic acid. *J. Colloid Sci.* **1950**, *5* (2), 115–139.
- (68) Katchalsky, A.; Eisenberg, H. Molecular weight of polyacrylic and polymethacrylic acid. *J. Polym. Sci.* **1951**, *6*, 145–154.
- (69) Pipe, C. J.; Majmudar, T. S.; McKinley, G. H. High shear rate viscometry. *Rheol. Acta* **2008**, *47* (5–6), 621–642.
- (70) Schneider, C. A.; Rasband, W. S.; Eliceiri, K. W. NIH Image to ImageJ: 25 years of image analysis. *Nat. Methods* **2012**, *9* (7), 671–675.
- (71) Entov, V. M.; Yarin, A. L. Influence of elastic stresses on the capillary breakup of jets of dilute polymer solutions. *Fluid Dyn.* **1984**, *19* (1), 21–29.
- (72) Yarin, A. L. *Free Liquid Jets and Films: Hydrodynamics and Rheology*; Longman Scientific & Technical: 1993.
- (73) Bazilevsky, A.; Entov, V.; Rozhkov, A. Liquid filament microrheometer and some of its applications. In *Third European Rheology Conference and Golden Jubilee Meeting of the British Society of Rheology*; Elsevier: Edinburgh, UK, 1990; pp 41–43.
- (74) Entov, V. M.; Hinch, E. J. Effect of a spectrum of relaxation times on the capillary thinning of a filament of elastic liquid. *J. Non-Newtonian Fluid Mech.* **1997**, *72*, 31–54.
- (75) Bazilevskii, A. V.; Entov, V. M.; Rozhkov, A. N. Breakup of an Oldroyd liquid bridge as a method for testing the rheological properties of polymer solutions. *Polym. Sci. A* **2001**, *43* (7), 716–726.
- (76) Bazilevsky, A. V.; Entov, V. M.; Rozhkov, A. N. Breakup of a liquid bridge as a method of rheological testing of biological fluids. *Fluid Dyn.* **2011**, *46* (4), 613–622.
- (77) Stelter, M.; Brenn, G.; Yarin, A. L.; Singh, R. P.; Durst, F. Investigation of the elongational behavior of polymer solutions by means of an elongational rheometer. *J. Rheol.* **2002**, *46* (2), 507–527.
- (78) Christanti, Y.; Walker, L. M. Surface tension driven jet break up of strain-hardening polymer solutions. *J. Non-Newtonian Fluid Mech.* **2001**, *100* (1–3), 9–26.
- (79) Christanti, Y.; Walker, L. M. Effect of fluid relaxation time of dilute polymer solutions on jet breakup due to a forced disturbance. *J. Rheol.* **2002**, *46* (3), 733–748.
- (80) Anna, S. L.; McKinley, G. H. Elastocapillary thinning and breakup of model elastic liquids. *J. Rheol.* **2001**, *45* (1), 115–138.
- (81) Rodd, L. E.; Scott, T. P.; Cooper-White, J. J.; McKinley, G. H. Capillary break-up rheometry of low-viscosity elastic fluids. *Appl. Rheol.* **2005**, *15* (1), 12–27.
- (82) Fuoss, R. M.; Strauss, U. P. Polyelectrolytes. II. Poly-4-vinylpyridonium chloride and poly-4-vinyl-N-n-butylpyridonium bromide. *J. Polym. Sci.* **1948**, *3* (2), 246–263.
- (83) Fuoss, R. M. Polyelectrolytes. *Discuss. Faraday Soc.* **1951**, *11*, 125–134.
- (84) Witten, T. A.; Pincus, P. Structure and viscosity of interpenetrating polyelectrolyte chains. *EPL* **1987**, *3* (3), 315.
- (85) Oelschlaeger, C.; Coelho, M. C. P.; Willenbacher, N. Chain flexibility and dynamics of polysaccharide hyaluronan in entangled solutions: a high frequency rheology and Diffusing Wave Spectroscopy study. *Biomacromolecules* **2013**, *14* (10), 3689–3696.
- (86) Uzum, C.; Christau, S.; von Klitzing, R. Structuring of Polyelectrolyte (NaPSS) Solutions in bulk and under confinement as a function of concentration and molecular weight. *Macromolecules* **2011**, *44* (19), 7782–7791.
- (87) Uematsu, Y.; Araki, T. Electro-osmotic flow of semidilute polyelectrolyte solutions. *J. Chem. Phys.* **2013**, *139* (9), 094901.

- (88) Cohen, J.; Priel, Z. Intrinsic viscosity of polyelectrolyte solutions. *Polym. Commun.* **1989**, *30* (7), 223–224.
- (89) Eisenberg, H.; Pouyet, J. Viscosities of dilute aqueous solutions of a partially quaternized poly-4-vinyl pyridine at low gradients of flow. *J. Polym. Sci.* **1954**, *13* (68), 85–91.
- (90) Roure, I.; Rinaudo, M.; Milas, M.; Frollini, E. Viscometric behaviour of polyelectrolytes in the presence of low salt concentration. *Polymer* **1998**, *39* (22), 5441–5445.
- (91) Ashok, B.; Muthukumar, M. Crossover Behavior of the Viscosity of Dilute and Semidilute Polyelectrolyte Solutions. *J. Phys. Chem. B* **2009**, *113* (17), 5736–5745.
- (92) Muthukumar, M. Theory of viscoelastic properties of polyelectrolyte solutions. *Polymer* **2001**, *42* (13), 5921–5923.
- (93) Wyatt, N. B.; Liberatore, M. W. Rheology and viscosity scaling of the polyelectrolyte xanthan gum. *J. Appl. Polym. Sci.* **2009**, *114* (6), 4076–4084.
- (94) Krause, W. E.; Tan, J. S.; Colby, R. H. Semidilute solution rheology of polyelectrolytes with no added salt. *J. Polym. Sci., Part B: Polym. Phys.* **1999**, *37* (24), 3429–3437.
- (95) Prini, R. F.; Lagos, A. E. Tracer diffusion, electrical conductivity, and viscosity of aqueous solutions of polystyrenesulfonates. *J. Polym. Sci., Part A: Gen. Pap.* **1964**, *2* (6), 2917–2928.
- (96) Cohen, J.; Priel, Z. Viscosity of dilute polyelectrolyte solutions: temperature dependence. *J. Chem. Phys.* **1990**, *93* (12), 9062–9068.
- (97) Cohen, J.; Priel, Z.; Rabin, Y. Viscosity of dilute polyelectrolyte solutions. *J. Chem. Phys.* **1988**, *88* (11), 7111–7116.
- (98) Oostwal, M. G.; Blees, M. H.; De Bleijser, J.; Leyte, J. C. Chain self-diffusion in aqueous salt-free solutions of sodium poly(styrenesulfonate). *Macromolecules* **1993**, *26* (26), 7300–7308.
- (99) Chen, S. P.; Archer, L. A. Relaxation dynamics of salt-free polyelectrolyte solutions using flow birefringence and rheometry. *J. Polym. Sci., Part B: Polym. Phys.* **1999**, *37* (8), 825–835.
- (100) Dou, S.; Colby, R. H. Charge density effects in salt-free polyelectrolyte solution rheology. *J. Polym. Sci., Part B: Polym. Phys.* **2006**, *44* (14), 2001–2013.
- (101) Lopez, C. G.; Rogers, S. E.; Colby, R. H.; Graham, P.; Cabral, J. T. Structure of sodium carboxymethyl cellulose aqueous solutions: A SANS and rheology study. *J. Polym. Sci., Part B: Polym. Phys.* **2015**, *53* (7), 492–501.
- (102) Krause, W. E.; Bellomo, E. G.; Colby, R. H. Rheology of sodium hyaluronate under physiological conditions. *Biomacromolecules* **2001**, *2* (1), 65–69.
- (103) Wyatt, N. B.; Liberatore, M. W. The effect of counterion size and valency on the increase in viscosity in polyelectrolyte solutions. *Soft Matter* **2010**, *6* (14), 3346–3352.
- (104) Konop, A. J.; Colby, R. H. Polyelectrolyte charge effects on solution viscosity of poly (acrylic acid). *Macromolecules* **1999**, *32* (8), 2803–2805.
- (105) Chen, Y.-J.; Steen, P. Dynamics of inviscid capillary breakup: collapse and pinchoff of a film bridge. *J. Fluid Mech.* **1997**, *341*, 245–267.
- (106) Day, R. F.; Hinch, E. J.; Lister, J. R. Self-similar capillary pinchoff of an inviscid fluid. *Phys. Rev. Lett.* **1998**, *80* (4), 704–707.
- (107) Rayleigh, L. On the capillary phenomenon of jets. *Proc. R. Soc. London* **1879**, *29*, 71–97.
- (108) Papageorgiou, D. T. On the breakup of viscous liquid threads. *Phys. Fluids* **1995**, *7*, 1529–1544.
- (109) Haward, S. J.; Sharma, V.; Butts, C. P.; McKinley, G. H.; Rahatekar, S. S. Shear and extensional rheology of cellulose/ionic liquid solutions. *Biomacromolecules* **2012**, *13* (5), 1688–1699.
- (110) James, D. F.; Sridhar, T. Molecular conformation during steady state measurements of extensional viscosity. *J. Rheol.* **1995**, *39* (4), 713–724.
- (111) Prabhakar, R.; Gadkari, S.; Gopesh, T.; Shaw, M. J. Influence of stretching induced self-concentration and self-dilution on coil-stretch hysteresis and capillary thinning of unentangled polymer solutions. *J. Rheol.* **2016**, *60* (3), 345–366.
- (112) Prabhakar, R.; Sasmal, C.; Nguyen, D. A.; Sridhar, T.; Prakash, J. R. Effect of stretching-induced changes in hydrodynamic screening on coil-stretch hysteresis of unentangled polymer solutions. *Phys. Rev. Fluids* **2017**, *2* (1), 011301.
- (113) Zebrowski, B. E.; Fuller, G. G. Rheo-Optical Studies of Polyelectrolyte Solutions in Simple Shear Flow. *J. Rheol.* **1985**, *29* (6), 943–954.
- (114) Cross, M. M. Rheology of non-Newtonian fluids - A new flow equation for pseudoplastic systems. *J. Colloid Sci.* **1965**, *20* (5), 417–437.
- (115) Bird, R. B.; Armstrong, R. C.; Hassager, O. *Dynamics of Polymeric Liquids*, 2nd ed.; John Wiley & Sons: New York, 1987; Vol. 1.
- (116) Arnolds, O.; Buggisch, H.; Sachsenheimer, D.; Willenbacher, N. Capillary breakup extensional rheometry (CaBER) on semi-dilute and concentrated polyethyleneoxide (PEO) solutions. *Rheol. Acta* **2010**, *49* (11–12), 1207–1217.
- (117) Sachsenheimer, D.; Hochstein, B.; Willenbacher, N. Experimental study on the capillary thinning of entangled polymer solutions. *Rheol. Acta* **2014**, *53* (9), 725–739.
- (118) Pincus, P. Excluded volume effects and stretched polymer chains. *Macromolecules* **1976**, *9* (3), 386–388.
- (119) Pincus, P. Dynamics of stretched polymer chains. *Macromolecules* **1977**, *10* (1), 210–213.
- (120) Clasen, C.; Plog, J. P.; Kulicke, W. M.; Owens, M.; Macosko, C.; Scriven, L. E.; Verani, M.; McKinley, G. H. How dilute are dilute solutions in extensional flows? *J. Rheol.* **2006**, *50* (6), 849–881.
- (121) Tiratmadja, V.; McKinley, G. H.; Cooper-White, J. J. Drop formation and breakup of low viscosity elastic fluids: Effects of molecular weight and concentration. *Phys. Fluids* **2006**, *18* (4), 043101.
- (122) Keller, A.; Odell, J. A. The extensibility of macromolecules in solution; a new focus for macromolecular science. *Colloid Polym. Sci.* **1985**, *263* (3), 181–201.
- (123) Ajdari, A.; Brochard-Wyart, F.; Gay, C.; De Gennes, P. G.; Viovy, J. L. Drag on a tethered chain moving in a polymer melt. *J. Phys. II* **1995**, *5* (4), 491–495.
- (124) Muthukumar, M.; Freed, K. F. Theory of concentration dependence of polymer relaxation times in dilute solutions. *Macromolecules* **1978**, *11* (5), 843–852.
- (125) Palangetic, L.; Reddy, N. K.; Srinivasan, S.; Cohen, R. E.; McKinley, G. H.; Clasen, C. Dispersity and spinnability: Why highly polydisperse polymer solutions are desirable for electrospinning. *Polymer* **2014**, *55* (19), 4920–4931.
- (126) Fang, Y.; Dulaney, A. D.; Gadley, J.; Maia, J. M.; Ellison, C. J. Manipulating characteristic timescales and fiber morphology in simultaneous centrifugal spinning and photopolymerization. *Polymer* **2015**, *73*, 42–51.